



**University of Dundee**

## **Strategic and practical guidelines for successful structured illumination microscopy**

Demmerle, Justin; Innocent, Cassandravictoria; North, Alison J.; Ball, Graeme; Müller, Marcel; Miron, Ezequiel; Matsuda, Atsushi; Dobbie, Ian M.; Markaki, Yolanda; Schermelleh, Lothar

*Published in:*  
Nature Protocols

*DOI:*  
[10.1038/nprot.2017.019](https://doi.org/10.1038/nprot.2017.019)

*Publication date:*  
2017

*Document Version*  
Peer reviewed version

[Link to publication in Discovery Research Portal](#)

### *Citation for published version (APA):*

Demmerle, J., Innocent, C., North, A. J., Ball, G., Müller, M., Miron, E., ... Schermelleh, L. (2017). Strategic and practical guidelines for successful structured illumination microscopy. *Nature Protocols*, 12(5), 988-1010. DOI: 10.1038/nprot.2017.019

### **General rights**

Copyright and moral rights for the publications made accessible in Discovery Research Portal are retained by the authors and/or other copyright owners and it is a condition of accessing publications that users recognise and abide by the legal requirements associated with these rights.

- Users may download and print one copy of any publication from Discovery Research Portal for the purpose of private study or research.
- You may not further distribute the material or use it for any profit-making activity or commercial gain.
- You may freely distribute the URL identifying the publication in the public portal.

### **Take down policy**

If you believe that this document breaches copyright please contact us providing details, and we will remove access to the work immediately and investigate your claim.

## Strategy and tactics for successful structured illumination microscopy

Justin Demmerle<sup>1,8</sup>, Cassandravictoria Innocent<sup>1,8</sup>, Alison J. North<sup>2</sup>, Graeme Ball<sup>1,3</sup>, Marcel Müller<sup>4</sup>, Ezequiel Miron<sup>1</sup>, Atsushi Matsuda<sup>5,6</sup>, Ian M. Dobbie<sup>1</sup>, Yolanda Markaki<sup>7</sup>, Lothar Schermelleh<sup>1</sup>

<sup>1</sup>Micron Advanced Bioimaging Unit, Department of Biochemistry, University of Oxford, Oxford OX1 3QU, UK

<sup>2</sup>Bio-Imaging Resource Center, The Rockefeller University, New York, NY 10065, USA.

<sup>3</sup>Current Address: Dundee Imaging Facility, School of Life Sciences, University of Dundee, Dundee, DD1 5EH, UK.

<sup>4</sup>Biomolecular Photonics Group, Faculty of Physics, Bielefeld University, Universitaetsstrasse 25, 33615 Bielefeld, Germany.

<sup>5</sup>Advanced ICT Research Institute Kobe, National Institute of Information and Communications Technology, Kobe 651-2492, Japan

<sup>6</sup>Graduate School of Frontier Biosciences, Osaka University, Osaka 565-0871, Japan

<sup>7</sup>David Geffen School of Medicine, Department of Biological Chemistry, UCLA, Los Angeles, CA 90095, USA

<sup>8</sup>These authors contributed equally to this work.

Correspondence should be addressed to L.S. (lothar.schermelleh@bioch.ox.ac.uk).

## EDITORIAL SUMMARY

This protocol describes calibration bead slide preparation, their use and additional strategies to reduce artifacts of structured illumination microscopy that will allow researcher to exploit the technique's full potential for biological applications.

## TWEET@MicronOxford

## ABSTRACT

Linear two- or three-dimensional structured illumination microscopy (SIM or 3D-SIM) enables multicolor volumetric imaging of fixed and live specimens with sub-diffraction resolution in all spatial dimensions. However the reliance of SIM on algorithmic post-processing renders it particularly sensitive to artifacts that may reduce resolution, compromise data and its interpretations, and drain resources in terms of money and time spent. Here we present a protocol that allows users to generate high quality SIM data while accounting and correcting for common artifacts. The protocol details preparation of calibration bead slides designed for SIM-based experiments, the acquisition of calibration data, the documentation of typically encountered SIM artifacts and corrective measures that should be taken to reduce them. It also includes a conceptual overview and checklist for experimental design and calibration decisions, and is applicable to any commercially available or custom platform. This protocol, plus accompanying guidelines, allows researchers from students to imaging professionals to create an optimal SIM imaging environment regardless of specimen type or structure of interest. The calibration sample preparation and system calibration protocol can be executed within 1-2 days.

**KEYWORDS:** structured illumination microscopy; 3D-SIM; artifacts; super-resolution imaging; microscope calibration.

## INTRODUCTION

Linear structured illumination microscopy (SIM, 3D-SIM) is a powerful and versatile method for generating three-dimensional super-resolution imaging data of biological structures with wavelength-dependent resolution down to ~100-130 nm in lateral dimensions<sup>1,2</sup> and ~280-350 nm in the axial dimension<sup>3,4</sup>. Its efficient optical sectioning capability, rapid multi-channel acquisition of live and fixed specimens, compatibility with widely used chemical and biological labels and commercial availability make SIM a popular choice among researchers, with hundreds of instruments being used worldwide. Increasingly easy-to-operate commercial systems have rendered the technique accessible to novice microscopists. However, to generate final super-resolution images the method relies heavily on complex mathematical algorithms and stringent system calibrations that are 'black boxes' to most users. This hidden technical complexity imposes an inherent risk of artifacts with varying degrees of impact that makes reproducibility, adaptation by users, and interpretation of biological conclusions difficult and can undermine confidence in the validity of SIM data<sup>5,6</sup>. The problem is compounded by the absence of widely available resources detailing these artifacts, their causes, and how to address them despite extensive publications detailing principles<sup>7,8</sup>, specific implementations<sup>9,10</sup> and biological applications<sup>11,12</sup> of SIM. Hence, this protocol is designed to facilitate the average researcher in any discipline, as well as imaging facility specialists, to make informed decisions about when and how to use SIM; how to create simple calibration samples to assess and monitor the performance of SIM systems; how to identify and correct for common errors in SIM imaging; and how to effectively present SIM data to the research community. The presented workflow for conducting SIM experiments and assessing data quality and validity should lower entry barriers for the average researcher and reinforce super-resolution microscopy as an essential tool of biological discovery.

### Artifact diagnosis and quality control

The increasing number of publications involving (3D-)SIM imaging illustrates the versatility and broad applicability of this method to address important aspects of biological research. However, SIM data presented in research publications commonly shows evidence of unreported artifacts that can be misinterpreted as biologically relevant features, potentially leading to false conclusions. In addition to these cases, experience shows that there is a much larger number of undocumented, unsuccessful imaging attempts, particularly when inadequately trained users are approaching the technique with pre-existing samples and without appropriate advice on experimental design and system setup.

Artifacts that may be frequently encountered in typical SIM imaging experiments (**Fig. 1**) include: fine ('hammerstroke') pseudo-structures originating from reconstructed non-modulated background/noise signal that intermixes with poorly resolved structural features (**Fig. 1b**, **Supplementary Fig. 1**); echo signals in axial direction of curved sample structures with different refractive properties ('lensing', **Fig. 1b'**); lateral striped extensions ('hatching') of features in one or more directions (**Fig. 1c**, **Supplementary Fig. 2**); repeated features ('ghosting') along the z-axis (**Fig. 1d**, **Supplementary Fig. 3**); fine hexagonal repeating ('honeycomb') pseudo-structures in areas of increased out-of-focus signal, especially in 2D-SIM images (**Fig. 1e**) or at the end planes of 3D-SIM image stacks (**Supplementary Fig. 4**); and transfer of signals from features located at opposite ends of the image stack ('z-wrapping') (**Supplementary Fig. 4**). These and other artifacts (a comprehensive list is provided in **Table 3**) often occur concomitant with a lower than expected increase in structural resolution in the lateral and/or axial direction. Attempts to counteract artifacts, either *ex ante* through conservative system hardware settings, and/or *post hoc* through computational filtering, results in images without the expected super-resolution increase, despite greatly improved contrast, thus resembling those obtained by standard widefield deconvolution microscopy. Thus it is important to perform quality control checks to confirm the effectively achieved structural resolution in the final reconstructed image, as well as the absence, or sufficient reduction, of artifacts. For an objective assessment of image resolution and data quality, we recommend *SIMcheck*, an open-source plugin for *ImageJ/Fiji* that provides a collection of raw and reconstructed SIM data checks together with specific calibration tools and useful post-processing utilities<sup>13</sup>. In this protocol, we use *SIMcheck* along with

specifically designed calibration slides as a first step in identifying artifacts and objectively quantifying system performance in order to make informed decisions on how to improve imaging and counteract artifacts.

### **Underlying principles**

The benefits of SIM, but also its susceptibility to specific artifacts, come from the fundamental concept of the method, which exploits interference effects between a fine striped illumination pattern and structures in the sample (analogous to Moiré interference). Through this ‘frequency mixing’, high spatial frequency components, corresponding to fine details in the sample that would otherwise escape detection, are shifted to collectable lower frequencies in the acquired image. This additional information can be computationally extracted and shifted back to the correct higher frequency before all available information is then recomposed in a linear reconstruction procedure to generate a super-resolution image with up to twice the spatial resolution in all axes (for details on the method see **Box 1**). The reconstruction algorithm operates in Fourier (frequency, reciprocal) space and relies on the optical transfer function (OTF), i.e. the Fourier transform of the point-spread function (PSF) that mathematically describes the microscope’s response to a fluorescent point source. It works under the premise that the detected light behaves in exactly the same way as in the acquired PSF used to create the OTFs. Therefore, any ‘mismatch’ between the OTF and the measured sample information will inevitably lead to artifacts of varying severity<sup>3</sup>. In addition to information from the structures of interest, SIM images will also contain information from other sources including optical aberrations in the sample, non-specific labeling, or noise, all of which can distort or obscure the structures of interest in the reconstructed image. Moreover, systematic aberrations can also be generated if the optical condition of the illumination pattern and its interaction with the sample are sub-optimal.

Importantly, practical achievement of the theoretical resolution enhancement depends profoundly on the contrast of the illumination stripes on the sample features. We generally refer to this as ‘modulation contrast’, which is determined both by the contrast properties of the labeled sample features and the optical properties and ‘stripe quality’ of the instrument<sup>13,14</sup> (**Fig. 2, Box 1**). In the extreme case of no modulation contrast, no interference (super-resolution information) is present and therefore resolution is not enhanced at all. In a more general case, if the modulation contrast is reduced, a smaller than expected fraction of the data can be derived from the high-frequency features, reducing contrast and decreasing super-resolution image quality and information content. Major contributions to this effect in biological samples are low contrast (signal-to-noise ratio, SNR), either inherent to the sample or from sub-optimal labeling, and spherical aberration caused by refractive index (RI) mismatch between the immersion media, mounting media, and the sample. The improvement of modulation contrast, by increasing specific signal intensity over non-specific background, and by optimizing RI matching through choice of immersion medium, is the aspect of SIM that the average user can perform relatively easy (since altering fundamental hardware and software properties is usually not possible) and is emphasized for that reason.

Consequently, there are two important principles to consider when designing and executing SIM experiments. The first, which is the main focus of this protocol, is to ensure that the illumination pattern is consistent, highly contrasted, optimally calibrated, and matching the OTF used for the mathematical reconstruction. This is accomplished by regularly confirming microscope calibration and by correcting for (depth dependent) spherical aberrations caused by RI mismatch between the coverslip, mounting medium and specimen. The second principle involves minimizing signal originating from sources other than the structure of interest, through careful experimental design and heightened standards for sample preparation and image acquisition. These aspects are discussed in the accompanying protocol by Kraus and colleagues<sup>15</sup>.

### **Overview of the procedure**

In addition to existing recommendations, experimental researchers have noted the need for a broad and accessible set of guidelines to improve experimental design, confirm instrument



calibration and assess image data quality<sup>16,17</sup>. While specifics may vary across system manufacturer, sample type, and the nature of the experiment, here we offer a calibration sample procedure, artifact diagnosis and reference tables as a roadmap to more accessible high-quality data collection and interpretation on a range of current SIM systems. As specified above, examples of the most common SIM-related artifacts are introduced to exemplify what the inexperienced user may encounter (**Fig. 1, Supplementary Figs. 1-4**). The critical concept of modulation contrast as a predictor and metric of SIM data quality is illustrated in **Fig. 2**, as maximizing this property in both system and sample is the goal of these calibration routines and the key to achieving reliable data.

Once these central issues are presented, the user is encouraged to re-evaluate the general imaging strategy in terms of microscopy technique, instrumentation and their suitability for addressing a specific biological research question (**Supplementary Fig. 5**), as these are fundamental choices. The calibration procedure and the overall experimental workflow from design to analysis (**Fig. 3**) indicate the necessary steps prior to main data acquisition to ensure high data quality and reproducibility. In addition, we offer a checklist of essential considerations at each stage in the process to facilitate experimental design refinement (**Supplementary Manual**) and provide a list of suitable fluorophores in **Table 1**.

The main procedure for assembling calibration slides and performing calibration checks are outlined in **Fig. 3b** and the slide preparation steps are illustrated in detail in **Fig. 4**. The expected results from these calibration slides are shown in **Fig. 5** and include selected examples of positive and sub-optimal outcomes, while recommendations for correcting errors in their preparation or imaging are listed in the troubleshooting sections (**Table 2**). Since a primary cause of SIM artifacts, and perhaps the most easily adjusted system parameter, is refractive index (RI) mismatch, a guide to matching RI between immersion media, reconstruction OTF, and sample is provided in **Fig. 6**. Additional illustrations and in-depth information to this critical aspect are presented in **Supplementary Figs. 6-9**. Further, an exhaustive list of SIM artifacts, their diagnostic readouts and potential countermeasures, can be found in **Table 3**. For specialists and developers of bespoke SIM systems, we provide an additional list of artifacts and diagnostics that are mainly associated with basic system setup and initial light path alignments (**Supplementary Table**) and show a practical example of beam misalignment detection using *SIMcheck* (**Supplementary Fig. 10**).

To aid novices in their understanding of these concepts, a discussion of fundamental principles of the SIM technique and image reconstruction in frequency space is provided in **Box 1**. Lastly, to work towards universal quality standards, we include a set of guidelines and criteria for data presentation and publishing (**Box 2**). These are designed to help experimenters, principle investigators, reviewers, and specialists involved in the publication process to ensure transparency, consistency, and reproducibility of the presented results. The protocol and recommendations are applicable to all commercially available and custom-built SIM systems, and add to the emerging range of open-source SIM-specific tools<sup>13,18,19</sup>.

### Level of expertise required

Any researcher or student familiar with generic wet-lab techniques and immunostaining may implement the calibration sample preparation protocol. No specific technical expertise is required to benefit from the experimental design and data presentation recommendations. Any researcher trained on a SIM instrument and familiar with recording data can implement the image acquisition, calibration data analysis, and quality control recommendations. Training of individual users in system calibration protocols requires experience in optical microscopy and ideally advanced technical knowledge of the imaging platform.

### Limitations

While this protocol should assist in improving the results of any SIM imaging experiment, it cannot overcome fundamental restrictions of the technique regarding resolution, photostability, or the limitations imposed by inherent properties of the specimen or the biomolecular target of interest. While the 2D or 3D resolution increase provided by SIM is sufficient to resolve a range of biologically significant macromolecular structures, any further increase in structural resolution,

i.e. below ~100 nm, requires diffraction unlimited super-resolution approaches such as non-linear (NL-) SIM<sup>20-22</sup>, stimulated emission depletion (STED) microscopy<sup>23-25</sup>, and single molecule localization microscopy (SMLM, e.g. PALM, STORM)<sup>26,27</sup>. These modalities, along with lower resolving techniques, such as widefield deconvolution or confocal laser scanning microscopy, are alternatives to SIM that should be considered during the experimental design phase of a project. In the case of SIM providing sufficient resolution to address a given research question, it may prove advantageous over other super-resolution techniques due to its straightforward capabilities for multi-channel, rapid, volumetric imaging and thereby provide additional benefits (**Supplementary Fig. 5a**).

Finally, it should be noted that this protocol does not ensure success for every possible sample. Certain specimens and biomolecular targets are too difficult (due to size, diffractive properties, dispersion, or label specificity) to image successfully even with these improved standards. Some biological and organic fluorophores do not have sufficient photostability to tolerate the repeated exposures of SIM (see **Table 1**). As with all super-resolution techniques, a compromise must be reached for each application between photodamage, imaging speed, information content (wavelengths, 3D volume, sample size, number of time points) and spatial resolution (effectively contrast-limited), all confined by the photon budget available (**Supplementary Fig. 5a** and **Supplementary Manual**). In practical terms, finding the balance between as high as possible contrast (i.e. by increasing target-specific signal and/or by decreasing non-specific background), while keeping acquisition bleaching rates acceptable is imperative for producing high quality SIM data (**Supplementary Fig. 5b**). Consequently, the limit of the method is reached if a minimum acceptable (modulation) contrast level is not achieved at all or without exceeding the critical threshold for bleaching.

## Experimental design

The most fundamental prerequisite to the successful application of any advanced imaging approach, including SIM, is the appropriate experimental design for a given biological question (**Fig. 3a**, **Supplementary Manual**). Design considerations for the sample include the choice of the specimen, the biological target(s) to be imaged, labeling strategy, mounting medium and imaging controls. Thicker specimens (over several tens of microns, such as whole-mount preparations or most tissue sections) are often impractical for SIM due to excessive spherical aberration, light scattering and out-of-focus blur, limiting stripe contrast and hence the ability to extract super-resolved information. Importantly, not all biomolecular targets are suitable for current super-resolution imaging approaches, such as highly mobile or transient binding factors, which move too rapidly and have insufficient spatial specificity to be cleanly resolved after reconstruction. Furthermore, the structures of interest should be of the size or distance range to benefit from SIM's resolution increase. Many macromolecular complexes and structures, such as centrosomes or replication clusters, are in the size range of 100-200 nm and can be well resolved with SIM. Of note, distances between differentially labeled (multicolor) targets can be determined with an accuracy in the 10-20 nm range, i.e. far below the optical resolution limit imposed by the microscope<sup>15,28</sup>. On the other end of the scale, if the biological question does not require the extended resolution provided by SIM or other super-resolution methods (such as when analyzing nuclear versus cytoplasmic localization), then conventional imaging methods will be easier and better suited for the endeavor (**Supplementary Fig. 5a**).

Live-cell SIM imaging requires that the dynamics of the structure of interest is sufficiently slow as to preclude movement during acquisition of one (3D) frame, which could cause motion artifacts. Due to the relatively low photostability of fluorescent protein tags, trade-offs are inevitable in terms of z-resolution, the number of time points and multi-color imaging restrictions, and thus will affect the experimental design. It is noteworthy that the acquisition speed is limited strongly by the method of illumination pattern formation (in descending order of speed: galvo-scanner array, spatial light modulator (SLM), mechanical grating) and the camera type (in descending order of speed: sCMOS, EMCCD, CCD) in different system setups. In this regard, the combination of 2D-SIM and TIRF has proven ideal for 1- and 2-color live cell imaging of cell surface dynamics with very high frame rates, but at the expense of imaging in 3D and restricted to the TIRF range of ~200 nm off the coverslip<sup>22,25,29</sup>.

**Hardware selection.** System hardware considerations cover mainly the choice of: objectives, camera type or mode, filter sets, and laser lines. Since commercial system setups are typically restricted in the choice of components for different applications, various strategic decisions may have to be taken when configuring a system for a desired application.

The standard oil-immersion objectives used for SIM should be independently checked for distortions of the PSF. High numerical aperture (NA) silicone-oil immersion objectives are superior for imaging larger z-volumes beyond 10-15  $\mu\text{m}$  in depth. The correction collar of these objectives must be adjusted precisely to allow matching of the imaging condition in the sample with the OTF set, analogous to changing the RI of the immersion oil. Once set, since the RI of the mounting medium of the biological specimen (typically in the range of 1.37-1.39) is close to that of the silicone immersion oil (RI of 1.40), distortion effects from refractive index mismatches become negligible, and thus, light scattering rather than spherical aberration becomes the limiting factor. The trade-offs in this case are reduced maximum resolution and brightness due to the lower NA of 1.30 (60x) or 1.35 (100x) silicone objectives compared to traditional oil objectives with NAs of up to 1.42.

sCMOS cameras have significant advantages over CCD or EMCCD cameras regarding read-out speed and field-of-view size. When camera read-out speed is the limiting factor, sCMOS detectors are the superior choice for fast (live-cell) acquisition when combined with fast illumination pattern generation (via a SLM or galvo-scanner array). The advantage of EMCCD cameras is the superior quantum efficiency and noise characteristics. Importantly, EMCCD cameras operated in conventional CCD mode are superior to sCMOS detectors in contrast-limited, but not photon-limited, imaging conditions. Such circumstances occur when densely labeled features extend within a larger volume in axial direction thereby strongly increasing out-of-focus blur (e.g. stained DNA in a cell nucleus). In comparison to sCMOS, the many-fold larger well-depth of CCD detectors allow a much higher dynamic range, increasing the modulation contrast in the image and ultimately improving the reconstructed data quality (**Fig. 2**). Finally, fast read-out modes increase the camera read-out noise and should only be considered for very fast live-cell imaging applications as the disadvantage of higher detector noise for the reconstruction quality mostly outweighs the gain in speed.

The design and quality of dichroic mirrors and emission filters is critical not only for the detection efficiency and specificity, but also for structured illumination pattern generation. Poor design or damage can significantly affect pattern quality and consistency among various angle and phase positions.

The range of available laser lines is relevant for the versatility and application range of the SIM system. Of note, short wavelength excitation with 405 nm offers not only the advantage of a higher resolution (down to 90 nm in xy) but also features a broader 'safe zone' of z-range where ghosting artifacts from spherical aberration remain below a reasonable threshold (**Supplementary Fig. 7**). Using the calibration and OTF generation procedures described here, combined with labeling by sufficiently bright and photostable dyes (e.g., DyLight405 or CF405M/S), should overcome the current limitations of short wavelengths for fixed cell applications.

**Fluorophore selection.** 3D-SIM imposes less strict requirements on the photophysics of dyes than its counterpart super-resolution techniques, STED and single molecule localization microscopy. Hence, a wide variety of fluorophores and dyes have been successfully used in different SIM applications and systems. Despite being considered the least demanding amongst all super-resolution methods (by relying in principle on widefield illumination and efficient CCD/CMOS detection, and not pushing resolution as much), SIM and particularly 3D-SIM still have a significantly higher demand on the available photon budget compared to widefield deconvolution microscopy, requiring up to 30-fold the number of acquisitions per 3D frame (5 phase steps, 3 angles, 2-fold z-sampling). Thus, the main criteria in fluorophore selection are brightness and photostability of the dye, as well as appropriateness for the laser line and filter set of the SIM system (**Table 1**). First-generation dyes like FITC and TRITC are significantly more prone to bleaching and are not recommended. Careful selection of a mounting medium

containing an anti-fade agent compatible with the chosen fluorophores is essential. Imaging of fluorescent protein (FP) tags may be more difficult and depends on expression levels, distribution, and structure of the tagged protein to be imaged, with sample-specific out-of-focus blur levels often limiting contrast. For fixed-cell applications, the GFP signal can be enhanced with GFP-specific antibodies. Single chain camelid antibody fragments (nanobodies) specific to GFP<sup>30</sup> and directly conjugated to more photostable dyes, such as ATTO 488 or Alexa 488, are useful due to particularly high affinity and low background. The red fluorescent proteins mRFP and mCherry are typically too dim and bleaching-prone for 3D-SIM imaging without such post-detection. For live-cell applications small self-labeling protein tags such as SNAP-tag or HaloTag can be a superior alternative if combined with tailored cell permeable fluorescent or fluorogenic organic dyes<sup>30,31</sup>.

SIM imaging of far-red emitting dyes may demand an adapted system configuration to adjust the first order beam positioning in the back aperture. Additionally some far-red fluorophores, like Alexa Fluor 647 or Cy5 exhibit pronounced reversible dark state switching in Vectashield<sup>32</sup> and thus require alternative mounting mediums (such as ProLong Diamond, under non-hardening conditions). Alternatively, if non-super-resolved widefield information is sufficient, far-red dyes can be imaged in the conventional mode, deconvolved and overlaid with SIM images.

System configuration and acquisition order also affect how the sample is bleached. In particular, high-sensitivity detection allows for shorter exposure times, thereby reducing bleaching effects. Finally, acquiring full stacks for each angle consecutively (typical for systems using a rotating phase grating) is more prone to bleaching artifacts than if the stack were acquired with angles interlaced, per each z-plane (as in systems equipped with galvo arrays or SLMs).

**Imaging controls.** Heightened technical standards will improve the final images from any experiment, but drawing meaningful conclusions from the data also requires appropriate controls. First, many studies seek to observe ‘colocalization’ of signals in two or more channels. However, super-resolution imaging has demonstrated that the concept of ‘colocalization’ is in many ways outdated; even when two targets are in biologically significant spatial proximity, frequently signals will not overlap<sup>33</sup>. Therefore, multi-channel co-localization or distance analyses should be supplemented by dual-color labeling of the same targets to provide technical baseline levels of signal separation<sup>34</sup>. Second, if possible, genetically encoded fluorophore localization should be confirmed with antibody labeling and vice versa, as a control for non-specific background that can easily lead to false-positive signals. If the absolute number of targets or foci is important to the experiment, a control with a non-specific fluorophore (such as only secondary antibody labeling or free GFP) can be used to establish a baseline for background signals. Third, as numerical quantification of imaging experiments is always preferred to illustrative single examples, a sufficient number of technical and biological replicates (generally no less than 10 and 3, respectively) should be analyzed. Finally, it is advisable for some applications to include fiducial marker of defined sizes, to compare with features of interest. While this is challenging, recent protocols for DNA origami provide a useful example of highly customizable *in situ* controls for both, absolute (single or multicolor) distance measurements and fluorophore density<sup>35</sup>.

### **System calibration & validation of system performance.**

For system calibration we recommend the use of five separate calibration slides utilizing various types of synthetic fluorescent beads (**Fig. 4, Fig. 5**). The first calibration slide presents a mix of up to four different color PSF-beads in optimal density to accommodate convenient acquisition of channel-specific PSF/OTF sets acquired with the same immersion medium (**Fig. 5a**). Next, three (or more) slides present monolayers of ~100-nm (sub-diffraction) diameter beads of different wavelengths matching the range of the system (i.e. 405 nm, 488 nm, 568/594/640 nm). Following the protocol below, these monolayers should be evenly distributed over the entire coverslip surface while leaving intermittent patches of bead-free background regions with a few isolated beads (**Fig. 5c**). These should be used as reference slides to determine system

parameters (line spacing, strip rotation ( $k_0$ ) angle), as well as to validate system alignment (phase and z-modulation; 1<sup>st</sup> and 2<sup>nd</sup> order beam position), and system performance by measuring the practically achievable resolution, confirming stability of performance over time, and assessing the quality of new parameter settings or new OTFs. The final calibration slide is for 3D channel alignment with a dual-layer preparation of 200-nm-Tetra Speck beads attached at appropriate density on both coverslip and the slide surface, separated by a layer of glycerol (**Fig. 5b**). Alternatively, multicolor click-labeled replication foci in mammalian cell nuclei can serve as an ideal biological calibration reference, and are described, along with ways to achieve optimal 3D color-channel alignment for multiple cameras using open-source software solutions (e.g., *Chromagnon*; <https://github.com/macronucleus/chromagnon>), in a protocol by Kraus and colleagues also published in this issue<sup>15</sup>.

As previously outlined, maximizing modulation contrast is essential to generate high-quality SIM data. This begins with the structured illumination pattern generated by the microscope optics, and therefore system calibration is of paramount importance. Regular checks of system performance are necessary, as the pattern generation systems are delicate, and even minor disturbances in the optical path can have significant effects on reconstruction quality. This spans rather technical concerns such as the alignment of the axial modulation maximum (hereby referred to as z-modulation) with the image plane (specific for 3D-SIM), to seemingly trivial issues such as dust on the optical components or fingerprints on the back of the objective. Once these issues are resolved, most artifacts can be localized to deficiencies in sample preparation or image acquisition.

The majority of SIM experiments are performed on commercial platforms from one of three suppliers: GE Healthcare's OMX; Zeiss's Elyra; or Nikon's N-SIM systems. While sharing the fundamental approach to SIM acquisition and reconstruction, each system (or in the case of OMX platforms, different versions) has a unique approach to both generating the structured illumination pattern and to reconstructing data. These differences can result in system-specific artifacts and limitations, and should always be considered before starting a SIM imaging experiment. A useful comparison of commercially available SIM systems used with the same biological sample type is available<sup>36</sup>, but the type of system accessible will generally be out of the control of the average user.

Optimization of the imaging system is critical and includes characterizing the point-spread behavior of the system, temperature dependence, chromatic aberration, and mechanical particulars such as stage drift or camera positioning. While service engineers will set up, initially calibrate, and annually maintain commercial SIM platforms, it is critical for advanced users or facility managers to perform basic calibration procedures independently and regularly check for performance drift over time. Moreover, procedures such as checking the uniformity and z-modulation of the illumination pattern, characterizing the PSF of the objective, and checking reconstruction quality with bead samples are necessary for any new optical configuration, and should be performed regularly even with commercial systems to maintain consistency in data collection and provide evidence of suboptimal alignment in preparation for service visits.

**OTF generation & matching to sample acquisition.** SIM reconstruction algorithms use the OTF that mathematically describes the microscope's response to a fluorescent point source (see **Box 1**). Commercial SIM systems will visually represent the OTF in different ways, and provide different methods for OTF generation. Besides the general optical properties of the system (wavelengths, magnification, NA, etc.) the OTF also encodes information on the level of spherical aberration and the modulation contrast of the structured illumination pattern. Thus, matching OTF and sample characteristics is a key goal in the acquisition process in order to keep artifacts below an acceptable threshold of detection (**Supplementary Figs. 7, 8**). There are several considerations for this process.

Firstly, spherical aberrations occur when light rays that strike a lens (or any other optical element) near the edge of the lens do not meet with rays passing through the center of the lens. While most high-end microscope objectives are corrected for spherical aberrations, the corrections only hold under ideal conditions, including a coverslip thickness of 170  $\mu\text{m}$  and a perfect match of refractive index (RI,  $n$ ) of the sample and the RI of the immersion oil (or

immersion medium, if not oil) ( $n_{oil}$ ) (**Supplementary Fig. 9a**). Thus, the sample needs to be regarded as an integral part of the optical system. When spherical aberrations are minimized such that all light rays intersect in the same ‘diffraction limited’ spot, the respective PSF has a symmetrical hourglass appearance, when viewed axially (**Fig. 5a**). This shape will deviate under sub-optimal conditions; it will become asymmetric towards the coverslip (bottom-heavy, if displayed in the orientation with coverslip at the lower end) if  $n_{oil}$  is higher than the optimum, and become asymmetric in the other direction (top-heavy), if the  $n_{oil}$  is lower than the optimum (**Fig. 6**). One important variable is the wavelength of the exciting and emitted light ( $\lambda_{ex/em}$ ) traveling to and from the fluorophore. Of note, instruments are typically calibrated for an intermediate excitation wavelength of 488 nm. Shorter and longer wavelengths will be diffracted at a smaller or wider angle, respectively. Hence any optimization must include considerations of the laser line to be used, particularly for multicolor image acquisitions (**Fig. 6**). For any target away from the coverslip surface, as in most typical biological applications, the RI of the sample (or more specifically the biological specimen with its surrounding mounting medium) becomes a key factor: the larger the mismatch between the RI of the immersion medium and the RI of the sample, the larger the degree of aberration with increasing z-depth. As it affects the density and thus the effective RI of both oil and mounting medium, the temperature (T) needs to be considered as well. Typically the nominal RI of immersion oil is indicated for 23 °C room temperature, while deviations thereof decrease or increase the effective RI of the immersion oil if the temperature is higher (e.g. for live cell observations) or lower, respectively (**Supplementary Fig. 9b**). The adverse effects can be compensated by either adapting the RI of the immersion oil, or by changing the correction collar of the objective (if applicable).

Secondly, optical aberrations introduced by elements in the light paths, such as lenses and dichroic filters, affect the measured OTF, which can substantially deviate from a theoretical OTF solely based on the parameters of the objective alone. Hence well-matched and empirically derived OTFs measured for individual channels will typically yield superior reconstruction results to a theoretical OTF. Thirdly, the effect of the z-modulation is also encoded in the reconstruction OTF, and is also dependent on the RI with which the OTF was recorded. This is why different combinations of RIs used for acquisition and reconstruction yield variable final results, with the higher mismatches generating worse reconstructions, as seen in a matrix of varying sample and OTF RIs (**Supplementary Fig. 8**). Instabilities of the z-modulation position over time should be monitored, and can be compensated by measuring a newer, matching, OTF. Finally, high noise levels in the OTF will translate into a prominent high-frequency noise component in the reconstructed image, just as does high noise in the underlying data (**Fig. 1b**, **Supplementary Fig. 1**). Thus it is important to acquire both PSF and sample raw data with a reasonably high dynamic range but without saturating the detector (ideally, using over 2/3 of the available CCD/sCMOS camera detector range). Laser power and camera exposure times for PSF and sample acquisition should be adjusted to achieve the optimal trade-off between high dynamic range and still acceptable photobleaching. Exposure times for fixed cell applications should typically be in the range of 20-100 ms to reduce intensity fluctuations and avoid potential mechanical drift artifacts.

In conclusion, matching a dataset acquired under less favorable sample conditions with an OTF that is acquired under the same suboptimal conditions will result in better reconstruction than by using an OTF acquired under ‘ideal’ conditions (**Fig. 6**, **Supplementary Figs. 6-8**). This becomes particularly relevant when combining OTFs for multicolor acquisitions that will necessarily impose less favorable conditions for wavelengths away from the reference wavelength. The diagrams shown in **Fig. 6** and **Supplementary Fig. 9c-e** provide general guidelines for how to adapt to different imaging conditions and different systems.

**Image reconstruction.** Given the robust (and often proprietary) nature of SIM reconstruction algorithms, the user’s ability to improve data post-acquisition is relatively limited. However, the adjustment of certain parameters, most prominently the high-frequency noise (Wiener) filter, can compensate for underlying deficiencies in the raw data by reducing noisy high-frequency components in the reconstructed image. The optimal filter setting for a given dataset can be estimated from the average *modulation contrast to noise ratio* (MCNR), one of several readout

metrics of *SIMcheck* (**Fig. 2, Supplementary Fig. 1**). Other parameters may include a (typically auto-estimated) weighting factor for the relative contribution of 1<sup>st</sup> and 2<sup>nd</sup> order information to the reconstruction, camera offset (dark frame and gain correction), and apodization factor that adjusts the systems input intensity profile. The angle directions ( $k_0$ ), and (2<sup>nd</sup> order) stripe width of the illumination must be predefined, either as starting parameter for an initial fitting and refinement procedure, or optionally as a fixed parameter if too few sample features or too little stripe contrast make reliable fitting improbable. Incorrect parameter settings or fitting errors can cause severe ‘hatching’ artifacts in affected directions (**Fig. 1c**) and should be carefully monitored, typically through warnings in the reconstruction log file. Relevant reconstruction parameters should be documented (e.g. in a log file) to facilitate comparison of temporally distinct data sets. Perhaps the most common oversight in reconstruction is the discarding of negative values (thresholding) in the reconstructed data, which severely reduces the ability of the experimenter to visually identify true signal from reconstruction artifacts (see **Table 3**), and also deprives the user of the possibility to obtain quantitative measures of the reconstructed data quality, e.g. through *SIMcheck*’s *max-to-min ratio* (MMR) or *z-minimum variance* (ZMW) metrics. Several methods of correcting for artifacts computationally have been described, and these can improve image quality substantially<sup>18, 37-41</sup>, but often at the expense of spatial resolution. Thus, in order to explore the full potential of the technique there is no substitute for well informed and thorough procedures at each step in the imaging process.

## MATERIALS

### REAGENTS

- Chloroform (Sigma-Aldrich, cat. no. 132950)  
**! CAUTION** Chloroform is hazardous. Avoid direct contact and inhalation.
- Hydrochloric acid, 37 % (vol/vol) (Sigma-Aldrich, cat. no. 258148)  
**! CAUTION** Hydrochloric acid is hazardous. Avoid direct contact.
- Ethanol absolute (100 % (vol/vol); Merck Millipore, cat. no. 100983)  
**! CAUTION** Ethanol is flammable.
- Glycerol (>99.5% (vol/vol); Sigma-Aldrich, cat. no. 49770)
- FluoSpheres carboxylate-modified microspheres, 0.1  $\mu$ m blue fluorescent (350/440; ThermoFisher, cat. no. F8797)
- FluoSpheres carboxylate-modified microspheres, 0.1  $\mu$ m yellow-green fluorescent (505/515; ThermoFisher, cat. no. F8803)
- FluoSpheres carboxylate-modified microspheres 0.1  $\mu$ m red fluorescent (580/605; ThermoFisher, cat. no. F8801), blue (360/440) and deep-red (633/660) PS-Speck beads 0.17  $\mu$ m diameter (PS-Speck Microscope Point Source Kit, ThermoFisher, cat. no. P7220). Alternatively, Fluoro-Max 0.10  $\mu$ m blue fluorescent beads (ThermoFisher, cat. no. B100B) may be used instead of blue (360/440) PS-Speck beads  
**▲ CRITICAL STEP** For OTF generation, only these beads, among all tested alternatives, have the necessary photostability and brightness to avoid bleaching and create high-quality PSFs to use as input in OTF generation. Using conventional blue beads will result in lower-quality OTFs and thereby lower-quality reconstructions in the blue channel.
- TetraSpeck Fluorescent Microspheres 0.2  $\mu$ m diameter (ThermoFisher, cat. no. T7280)
- DV immersion oil kit containing ¼ oz. bottles of 18 oils with refractive indices 1.500 to 1.534 (GE Healthcare, cat. no. 29163068). Alternatively, Cargille Laboratories offers bulk ‘Laser Liquid’ customized to the refractive index requested.

### EQUIPMENT

- Structured illumination microscope (e.g., GE Healthcare OMX; Nikon N-SIM; Zeiss Elyra S.1)
- Ultrasonic waterbath sonicator (e.g., VWR Ultrasonic Bath)
- Fine-tip forceps (Dumont #5; Fine Science Tools, cat. no. 11251-20 or similar)
- Low protein binding 1.5 mL tubes with safe lock lid (Eppendorf, cat. no. 022431081)

- Coplin jars (ThermoFisher Scientific, cat. no. 107)
- Coverslip holder (mini-racks) (ProSciTech, cat. no. H447)
- Soft task wipes (e.g., Kimwipe, Kimberly-Clark Professional, cat. no. 34155)
- Cotton-tipped swabs for optical cleanup (Edmund Optics, cat. no. 56-926)
- Lens cleaning tissues (e.g., Whatman, GE Healthcare, cat. no. WHA2105862)
- Quick-drying nail polish, preferably bright colored metallic, or CoverGrip coverslip sealant (Biotium, cat. no. 23005)
- Borosilicate precision cover glasses, thickness No. 1.5H ( $170 \pm 5 \mu\text{m}$ ); 18x18 mm or 22x22 mm (e.g., Marienfeld Superior, cat. no. 0107032)
- Clean glass microscope slides (76x26 mm / cleaned packed in fiber-free boxes)
- Slide storage boxes (Pelco, cat. no. 2106)
- Unix or Windows 64-bit OS is preferred, with 32-bit systems acceptable but likely to show slow performance. Adequate storage capacities for the database setup are required, as well as 4 to 8 GB RAM and current multi-core processors.
- The *Fiji* distribution<sup>42</sup> of *ImageJ*<sup>43</sup> is recommended. Other *ImageJ* distributions must have the *BioFormats Importer* installed. All distributions should be the most up-to-date version.
- The *SIMcheck* plugin<sup>13</sup> for *ImageJ/Fiji* should be installed for quality control and assessment of raw and reconstructed 3D-SIM data. For 3D FFT functionality in the most current *SIMcheck* 1.1 version, the *Parallel FFTJ* plugin (<https://sites.google.com/site/piotrwendykier/software/parallelfftj>) must be installed.

## REAGENT SETUP

**1 M HCl:** add 7 ml concentrated HCl to 250 ml ddH<sub>2</sub>O. Store at room temperature, stable for several months.

**70% (vol/vol) EtOH:** mix 15 ml ddH<sub>2</sub>O + 35 ml Ethanol absolute in a 50 ml self-standing Falcon tube or suitable dispenser; used for microscope slide cleaning. Store at room temperature, stable for several months.

**Chloroform:** aliquot into 50 ml Duran glass bottle; used for microscope slide and objective cleaning. Store at room temperature, stable for several months.

## EQUIPMENT SETUP

**Vortexes or sonicators.** Either benchtop vortexes or sonicators can be used interchangeably. However, if a waterbath sonicator is used, monitor the water temperature as it will rise over time and cause damage to carboxylate-modified beads.

## Structured Illumination Microscopy

The 3D-SIM system should be well aligned and calibrated by trained service engineers. For multi-camera systems, a channel alignment sample should be prepared. Consistent temperature in the imaging room or environment ( $23 \text{ }^{\circ}\text{C} \pm 5 \text{ }^{\circ}\text{C}$ , with  $< 0.5 \text{ }^{\circ}\text{C}$  variation/h) is recommended to avoid mechanical drift, variation in camera output, and changes in the refractive index of immersion oil and samples.

## PROCEDURE

### Pre-cleaning coverslips and slides ● TIMING 30 min

1| Place coverslips in a mini-rack and pre-clean for 30 min in a gently shaking beaker of 1 M HCl. Place slides in a coplin jar and follow the same procedure.

2| Rinse twice in ddH<sub>2</sub>O and transfer to a beaker (a coplin jar for slides) of 100% (vol/vol) EtOH for storage. Air dry prior to use.

▲ **CRITICAL STEP** Thorough cleaning of coverslips is essential for preparing calibration bead



slides. Dry slides and coverslips vertically or at an angle to avoid dust collection.

■ **PAUSEPOINT** Pre-cleaned coverslip can be stored for several months in 100% EtOH in a suitable sealed container (e.g. Petri dish sealed with Parafilm) preferably at 4 °C to prevent evaporation.

### **Preparation of PSF calibration slide ● TIMING 60 min**

3| Dilute 1 µl each of 0.1 µm 505/515 (green-yellow) and 580/605 (red) fluorescent carboxylate-modified microspheres in 98 µl ddH<sub>2</sub>O to make 100 µl pre-stock solution.

■ **PAUSEPOINT** Diluted microspheres can be stored at 4 °C for several weeks.

4| Add 0.5 µl of the pre-stock solution, 10 µl undiluted 0.17 µm 350/440 (blue) and 10 µl undiluted 0.17 µm 660/680 (far-red) fluorescent carboxylate-modified microspheres to 29.5 µl ddH<sub>2</sub>O to make 50 µl of the final stock solution.

■ **PAUSEPOINT** The microspheres can be stored at 4 °C for several weeks.

5| Sonicate stock solution for 10 min. Dilute 1 µl stock solution in 99 µl EtOH. Immediately apply 5 µl of this solution onto a pre-cleaned coverslip, spreading the droplet with the pipette tip, and air dry for at least 30 min. The final concentrations ( $1:10^6$  for green and red microspheres, 1:500 for blue and far-red microspheres) are chosen to average slightly less than one bead per field of view ( $256 \times 256$  pixels  $\triangleq$  field size of approx.  $20 \times 20$  µm with a pixel size of ~80 nm). Dilution ratios may have to be adapted depending on microsphere manufacturer or microscope configuration.

▲ **CRITICAL STEP** Homogenization of bead solution can be achieved with vortexing. However, sonication is preferred as it reduces the formation of aggregate pools as they dry.

▲ **CRITICAL STEP** Once bead solution has been applied to coverslips, allow this to dry, undisturbed and covered for 30-60 min. Use before drying may cause the beads to detach.

### **Preparation of bead layer calibration slides ● TIMING 30 min (concurrent)**

6| Sonicate 1 ml undiluted 0.1 µm fluorescent carboxylate-modified microspheres then transfer 1 µl to an Eppendorf tube. Use one tube each for blue, green-yellow, red and far-red microspheres, respectively.

7| Add 5 µl of EtOH absolute to the tube, depressing the pipette plunger once and immediately adding all 6 µl to the center of a pre-cleaned coverslip. Use the pipette tip to spread the liquid from the center while the EtOH evaporates, without pipetting up and down. Air dry for at least 20 min.

▲ **CRITICAL STEP** Work quickly. EtOH weakens the carboxylate-modified shells and these microspheres will disintegrate if handled roughly or left in alcohol. Additionally, the goal is to have contiguous patches of beads, ideally one bead-layer thick, to illustrate features of the structured illumination pattern. Spreading the microsphere droplet around the coverslip is critical to making flat patches of beads rather than clumps.

### **Preparation of 3D multicolor alignment bead slide ● TIMING 30 min**

8| Dilute 0.2 µm diameter TetraSpeck microspheres 1:20 in ddH<sub>2</sub>O and vortex for 1 min.

▲ **CRITICAL STEP** To ensure even distribution of beads for image acquisition, thorough vortexing is pivotal. Alternatively sonicate for 10 min in an ultrasonic waterbath.

9| Transfer 2 µl of the bead solution to an Eppendorf tube. Add 10 µl of EtOH absolute and without time delay gently pipette 6 µl the suspension on the middle of a pre-cleaned no. 1.5H coverslip from Step 2 and 6 µl of suspension on the center of a pre-cleaned slide. Gently streak out bead suspension onto coverslip and slide surfaces with the pipette tip.

10| Allow beads to dry for at least 20 min covered and protected from dust. (Alternatively, if

available, dry in a mini lab oven at 37 °C for 5 min.)

### **Final slide preparation ● TIMING 30 min**

**11|** For PSF and bead layer calibration slides, apply ~10 µl 100% (vol/vol) glycerol to the fully dried coverslip. Next, ready a labeled and pre-cleaned slide (frosting side down), or use non-frosted slides.

**12|** Using fine-tipped forceps, slowly lower the coverslip onto the slide, placing it at the center and taking care to avoid air bubbles.

**13|** Allow the glycerol to distribute evenly between the coverslip and slide. Press down gently with as soft task wipe to remove excess mounting medium at the edges. Seal carefully with nail polish or coverslip sealant.

**▲ CRITICAL STEP** For 3D-calibration slides this will typically produce bead layer distances of 5-10 µm between the two bead layers. Reducing the amount of glycerol below 10 µl may lead to the formation of air bubbles. Thus, if the distance between layers is larger, be more thorough in removing excess mounting medium at the edges. Thorough removal of excess medium also promotes hardening of the nail polish sealant, which is vital for long-term storage and repeated use of the sample.

**■ PAUSE POINT** Calibration slides can be kept for several days to weeks at 4 °C or for several months at -20 °C.

**14|** Before mounting calibration slides on the microscope, clean the coverslip surface with 70% (vol/vol) EtOH using soft task wipes, followed by 100% (vol/vol) chloroform, using an adhesive-free cotton swab or lens cleaning tissue.

### **Acquiring PSF/OTF sets. ● TIMING 2 hours (with practice)**

**15|** Mount the PSF slide (Steps 3-5) using the reference imaging oil with refractive index (RI) optimal for green emission.

**▲ CRITICAL STEP** The reference RI for green emission yields a symmetric PSF of green-emitting beads located on the coverslip. The reference RI for orange or red emission is typically shifted by one oil step (+0.002) with respect to the green reference. Once the reference RI is determined for a given system and a given ambient temperature, it remains constant for those conditions. Note that temperature shifts affect the refractive index of immersion media and thus need to be considered and appropriately corrected for (**Fig. 6, Supplementary Fig. 9**).

**16|** Find an area of the slide with isolated individual beads, and center a bead in the field of view such that no other beads are visible. The detector will report its highest count when the illumination focus is at the center of the bead. Incrementally adjusting the focus deeper/shallower into the bead (e.g., using z-steps of approx. 0.1 µm) will help to find the optimal midsection.

**17|** Acquire an 8 µm stack (+/-4 µm from the chosen bead center) with step-size 0.125 µm in widefield mode. Reviewing the intensity histogram of this stack, determine if the acquisition's dynamic range has reached as close as possible to the maximum bit depth of the camera (typically 14, 15 or 16-bit), without entering saturation. If saturated, reduce laser light intensity or exposure time as necessary, check there is no saturation with a single acquisition frame, and then acquire a new stack.

**18|** Assess widefield PSF for any variation, asymmetry, or astigmatism introduced by the objective or by air bubble(s) in the immersion medium by scrolling through the z-stack as well as inspecting the orthogonal view. For better visualization of dim features in the PSF, such as Airy rings, use gamma scaling 0.5 or lower (**Fig. 5a**).

**19|** Generate a series of OTFs from a bright bead using different acquisition angles. Assess the quality of each OTF visually (when possible) and empirically by reconstructing a bead layer dataset recorded in the same channel with the same RI oil and acquisition settings (Steps 22-24). For quantitative comparison of reconstruction quality, use MMR and ZMV metrics of *SIMcheck* (Step 29) (**Fig. 5e**). Repeat Steps 16-18 using the reference imaging oil with refractive index (RI) optimal for orange/red emission as required.

**20 |** Repeat Steps 15-19 for each objective as necessary.

**21|** When an optimal refractive index for the central wavelength has been determined, acquire one single-bead stack for OTF generation with the appropriate acquisition settings for the system in use (e.g. single-angle SI-PSF acquisition for OMX). This should be performed for all colors using the immersion oil with the refractive index that reflects the best trade-off in asymmetry between all channels, rather than using immersion oils with different refractive indices to acquire optimal PSFs for each channel. It is recommended to generate two OTF sets (multiple channel OTFs acquired with the same RI immersion oil): (1) using the reference immersion oil for the green channel, optimized for multicolor acquisition of blue and green fluorescence, and (2) using the optimal immersion medium for the orange/red channel (i.e. the OTF set acquired with a higher RI immersion oil). Optimizing for the orange/red channel is recommended for multicolor acquisitions involving the red and/or far-red channel due to the larger range of safe reconstructions in the blue and green emission channels (**Supplementary Figs. 7-9**).

#### **Illumination pattern checks ● TIMING 60 min**

**22|** Mount the bead-layer slide for the given wavelength, using the reference imaging oil (Step 15; **Fig. 6**).

**23|** Find a field containing even bead monolayer patches with intermittent bead-free background areas and occasional single beads. Empty areas will be important for accurate clipping offset and for determining the sample's z-minimum variance (ZMV). Adjust acquisition parameters accordingly to use the recommended bit depth of the camera while avoiding saturation.

**24|** Acquire a stack (in structured illumination mode) of the bead field. Usually a stack height of 4  $\mu\text{m}$  is sufficient.

**25|** Visually inspect the raw data. It should be free of particularly dark corners, noticeable aberrations, or extraneous patterns.

**26|** Open the raw data set in ImageJ/Fiji and use the 'Channel Intensity Profiles' tool in *SIMcheck*. Intensity should be near equal between phases (the spacing of data points) and roughly equal between angles (the difference between rows of data points). Some variation in intensity between angles is inevitable (due to factors like single- vs. multimode fiber-optic coupling or transmittance/absorbance characteristics of the dichroic mirror) but should be under 30%.

**27|** With the raw dataset enabled, select the 'Raw Data > Fourier Projections' function in *SIMcheck*. Confirm the presence of distinct first- and second-order spots in the Fourier transform. Using the mouse cursor, hover over the spot farthest from the center - ImageJ/Fiji will report the achieved resolution in  $\mu\text{m}/\text{cycle}$ . Absence of spots from the *SIMcheck* readout may indicate that initial diffraction spots were beyond the radius of the system's back focal plane by misalignment, leading to a low abundance of high order information assigned to the spatial domain. Alternatively, due to the Stokes shift of excitation and emission wavelengths, second order emission spots may escape the back focal aperture (e.g. if far-red excitation spots are positioned at the very edge of the aperture).

**28|** Apply the 'Illumination Pattern Focus' calibration tool in *SIMcheck*. If the channel-specific angle is known, enter this number. Else this angle can be derived from the raw dataset itself in drawing a line selection parallel to the contrast stripes. What is produced is a projected orthogonal view of the stripe pattern for each angle to assess the position of the 3D illumination pattern relative to the image plane. The axial modulation of the illumination should be consistent in all three angles. Ideally the maximum stripe modulation should be in line with the bead layer, thus showing a single layer of alternating bright and dark square-like sections across the field, rather than appearing as a 'zipper-like' double layer (**Fig. 5d**).

**29|** Perform the spherical aberration mismatch (SAM) check in *SIMcheck* and assess the value of the z-minimum variance (ZMV) statistic.

## **Reconstructing calibration datasets and quality control ● TIMING 1-2 hours**

**30|** Using the raw data collected in Step 24, and the channel-specific OTFs collected in Step 21, reconstruct the raw data using the commercial or open-source SIM reconstruction software of choice. For multicolor acquisitions (such as with experimental datasets), use a set of channel-specific measured OTFs acquired with immersion medium of the same refractive index  $n_{\text{oil}}$  (or  $n_{\text{silicone}}$ ) for all channels, optimizing either for the green/blue (2-color only) or for the red channel (for 2 and 3-color experiments including the red channel) as appropriate (**Fig. 6b**, **Supplementary Fig. 9**).

**31|** During the reconstruction step of processing calibration (and experimental) datasets, deactivate the option in the reconstruction software that ignores negative unsigned values in the image. This option is titled 'discard negatives' in GE's *SoftWoRx* and 'baseline cut' in Zeiss's *Zen* SIM reconstruction software, respectively.

▲ **CRITICAL STEP** *SIMcheck* reconstruction quality checks require non-thresholded (unclipped) data. Thresholding can be applied after quality control, e.g. using *SIMcheck*'s *Threshold and 16-bit Conversion* utility.

**32|** During the reconstruction step of processing calibration (and experimental) datasets, empirically determine a high-frequency noise (Wiener) filter setting appropriate for the data, using the Wiener filter setting recommendation in *SIMcheck*'s *Raw Modulation Contrast* tool, if applicable.

**33|** Assess reconstruction quality, check for artifacts (**Fig. 1**, **Fig. 2**), and proceed to acquisition and reconstruction of experimental samples.

## **● TIMING**

Steps 1-2, Pre-cleaning coverslips and slides: 30 min

Steps 3-5, Preparation of PSF calibration slides: 1 h

Steps 6-7, Preparation of bead layer calibration slides: 30 min, concurrent with steps 3-5

Steps 8-10, Preparation of multicolor alignment bead slide: 30 min, concurrent with steps 3-5

Steps 11-14, Final slide preparation: 30 min

Steps 15-21, Acquiring PSF/OTF sets: 2 h

Steps 22-29, Illumination Pattern checks: 1 h

Steps 30-33, Reconstruction and quality control of calibration datasets: 1-2 h

## **TROUBLESHOOTING**

Troubleshooting advice for the preparation of bead slides and acquisition of calibration data can be found in **Table 2**. An extended documentation and troubleshooting of various SIM-related artifacts is provided in **Table 3**. Troubleshooting advice for certain system alignment issues can be found in **Supplementary Table S1**.

## ANTICIPATED RESULTS

There are five (or more) calibration slides produced in this protocol: three (or more) dense bead slides with single-wavelength beads for each channel of the microscope, one dilute bead slide with multiple single-wavelength beads for acquisition of PSFs in multiple channels; one moderately dilute bead slide with multi-wavelength beads for multi-channel alignment. The PSF slide should have single sub-diffraction sized (0.1-0.17 $\mu$ m) beads, diluted sufficiently to obtain single beads per 256 x 256-pixel frame (**Fig. 5a**). This density allows for creation of experimental OTFs on GE systems; while other systems may require slightly different datasets for OTF creation, isolated PSFs are essential for determining the relative aberration of channel-specific PSFs in different immersion media and imaging conditions. The multi-channel alignment slide should have two parallel layers of intermediately dense TetraSpeck beads approx. 5-10  $\mu$ m apart to compensate for depth-related chromatic aberration (**Fig. 5b**). The bead layer slides should be dense enough to have uninterrupted patches of beads adjacent to isolated individual beads (**Fig. 5c, center**), while not too sparse (**Fig. 5c, left**) or overly dense (**Fig. 5c, right**). Running the 'Illumination Pattern Focus' function in *SIMcheck* will produce a projected view of lateral cross-section of the bead-layer slide along each angle in the raw data (**Fig. 5d**). This permits visual inspection of the modulation pattern, to confirm that all three angles show a consistent relative positioning of axial modulation and image plane (bead layer) to ensure matching with the OTF. If misaligned, a 'zipper' pattern is observable in the bead field (**Fig. 5d, top**) compared to a single bead layer with high contrasted (lateral) modulation (**Fig. 5d, bottom**). Check for various artifacts as shown, and consult the troubleshooting table to make appropriate adjustments before continuing on to image biological samples. The differences in reconstruction quality upon optimization of z-illumination (system-permitted) and optimized matching of OTFs (e.g. old and a newly generated) should be empirically and quantitatively determined by comparing reconstructions of bead layers and measuring MMR and ZMV metrics with *SIMcheck* (**Fig. 5e**). Finally, off-center beam misalignment can be identified by hatched pattern in out-of focus regions leading to spurious spots in the corresponding 3D-FFT that can be generated with the 'Reconstructed Fourier Plot' function in *SIMcheck* 1.1 (**Supplementary Fig. 10**).

## AUTHOR CONTRIBUTIONS

C.I., J.D., A.N., M.M., E.M., Y.M., and L.S. collected data and created figures. A.M., G.B., M.M., and I.D. provided technical expertise and advice. All authors contributed to artifact documentation. J.D., C.I., A.N., and L.S. wrote the manuscript. A.N., Y.M. and L.S. conceived the project.

## ACKNOWLEDGEMENTS

We acknowledge Jürgen Neumann and Michael Grange for technical support, and Leanna Ferrand of GE Healthcare for helpful discussion. The 2014 OMX User Meeting had notable contributions to the publication recommendations. We thank all colleagues that contributed in many discussions to shape this protocol. We are further indebted to Heinrich Leonhard and Ilan Davis for their long-standing support. This work was funded by the Wellcome Trust Strategic Awards 091911 and 107457 supporting advanced microscopy at Micron Oxford. The OMX 3D-SIM system in the Rockefeller University Bio-Imaging Resource Center was funded by Award Number S10RR031855 from the National Center For Research Resources. J.D. is supported by the NIH-Oxford-Cambridge Scholars Program. G.B. is supported by an MRC Next Generation Optical Microscopy Award (MR/K015869/1). A.M. is supported by JSPS KAKENHI Grant Numbers JP16H01440 ("resonance bio"), JP15K14500 and JP26292169.

## COMPETING INTERESTS

The authors declare no competing financial interest.

## TABLES

**Table 1** | List of recommended and less suitable fluorophores and fluorescent proteins for 3D-SIM applications. Fluorescent proteins are *italicized*. Note that the list is not exhaustive and that these recommendations are based on mounting in Vectashield.

Laser line	Recommended	Alternatives	Less suitable
405 nm	DyLight 405	CF405M, CF405S**	Alexa Fluor 405*
488 nm	Alexa Fluor 488 <i>mNeonGreen</i>	ATTO 488, DyLight 488, <i>EGFP</i>	FITC
532 nm	Alexa Fluor 532	Alexa Fluor 555, Cy3	TRITC
561 nm	Alexa Fluor 568, <i>TagRFP</i>	Alexa Fluor 546/555, Cy3	Rhodamine Red, <i>mRFP</i>
592 nm	Alexa Fluor 594	ATTO 594, DyLight 594	Texas Red, <i>mCherry*</i>
640 nm	ATTO 647N		Alexa Fluor 647*, Cy5*

\* Not suited for mounting in Vectashield but reported to work well in other mounting media. \*\* May photoconvert in other mounting media

**Table 2** | Protocol troubleshooting

Step	Problem	Reason for issue	Solution
7	Floating debris in bead layer slide	Bead slide is old, causing beads and monolayer fragments to detach and move inside the mounting medium.	Prepare a new bead lawn slide. Store in cool, dry location when not in use. Keep out of light, when possible.
	Beads too sparse	Beads dispersed too quickly to form monolayers.	Increase volume of undiluted bead stock solution. Use less ethanol when applying undiluted beads.
	Beads too dense	Beads were not dispersed quickly enough.	Reduce volume of undiluted bead stock solution. Use more ethanol when applying undiluted beads.
13	Bubbles in mounting medium	Too little mounting medium applied. Alternatively, drop of mounting medium applied contained bubbles when pipetted onto coverslip.	Small single bubble: scout a new area of your sample until a PSF bead with uniform airy rings can be found and acquired. Larger and multiple bubbles: apply mounting medium to center of coverslip without creating any bubbles and gently place coverslip directly atop droplet. The weight of the coverslip will allow the droplet to spread radially out towards coverslip edges. Only once all edges have been reached: remove excess mounting medium with gentle pressure from fingers, clean and seal. Alternatively, place tiny strips of torn filter paper (Whatman no. 4) against each edge of the coverslip and leave it for a couple of minutes to wick away excess mountant.
18	Crescent-shaped airy rings	Bubbles in immersion medium.	Remove slide, clean oil off objective with lens paper soaked in chloroform, clean coverslip accordingly and re-apply oil..
21	Sub-optimal OTFs	PSF airy ring contribution from multiple beads.	Check slides for bead density to ensure an 8 $\mu$ m thick, 256x256 px window can acquire a single PSF bead. Acquire PSFs of solitary, bright beads at different angles, then select the optimal OTF.

**Table 3 |** Artifact documentation

Figure	Artifact type	Possible cause	SIMcheck readout	Troubleshooting
1b, S1	High-frequency noise ('hammerstroke') pattern associated with lower than expected resolution improvement.	Low modulation contrast in the raw data due to: Inherently low contrast of the structure of interest, high out-of-focus blur contribution; Sample labeling too weak; Signal intensities (dynamic range) too low; High-frequency noise (Wiener) filter constant set too low.	<p><i>Raw Channel Intensity Profiles</i> Total intensity variation TIV &gt; 50%</p> <p><i>Reconstructed Intensity Histogram</i> Max-to-min ratio MMR &lt; 3</p> <p><i>Raw Modulation Contrast (Modulation Contrast Ratio, MCR &lt; 6 = recommended Wiener filter setting &gt; 0.0050**).</i></p> <p><i>Reconstructed Fourier Plots</i></p>	<p>[Sample] Chose suitable biological target/structure; revise labeling strategy; use brighter, more photostable dyes; reduce background caused by non-specific labeling and/or avoid auto-fluorescence by switching to orange/red dyes.</p> <p>[Acquisition] Increase dynamic range either by increasing laser power or exposure time until photobleaching becomes limiting. Reduce z-height, while making sure that first and last image plane are just out of focus (ideally no stripes should be visible). Choose region with reduced out-of-focus blur. Minimize squashing of extended structures along the optical axis by avoiding hardened mounting media (e.g. Movirol or cured ProLong Gold).</p> <p>[System] If photostability and timing considerations permit use camera mode with higher photon well depth (CCD &gt; EMCCD &gt; sCMOS); decrease gain (EMCCD); use lower read-out speed.</p> <p>[Recon] Increase Wiener filter constant to reduce frequency support matching to the lower raw data quality. <i>Note:</i> overly high filter constant (OMX &gt;0.0060) may generate hatch pattern artifacts and blurry images with reduced resolution.</p>
		PSF/OTF recorded with too low SNR.	OTF amplitude 'lobes' have frayed edges (OMX).	[System] Acquire channel-specific PSF/OTF with high dynamic range, while avoiding saturation or extensive exposure times (>200ms). If beads are too dim, prepare new bead sample on thoroughly cleaned #1.5H precision coverslips mounted with pure glycerol.
2b	(locally confined)	Reduced stripe modulation contrast in confined sample areas with high out-of-focus blur contribution.	<i>Modulation Contrast Map</i>	[Acquisition] Increase dynamic contrast in the raw data. If applicable, exclude image regions with substandard MCR from consideration/evaluation.
	Low axial (z) resolution	1 <sup>st</sup> order excitation beams are not positioned near the edge of the back-focal plane (BFP). (Note: axial frequency support may also vary	<i>Raw Fourier Projection</i> 2 <sup>nd</sup> order emission spots (close to the BFP edge) should be clearly detectable on high	[System] Test axial resolution of the objective by measuring the axial (xz) full width at half maximum (FWHM) of individual 100 nm beads (widefield and reconstructed SIM) in different color channels. If FWHM of reconstructed beads is

		between objectives, most notably through differences in the NA as z-resolution scales with NA <sup>2</sup> )	contrast (calibration) sample, with radial position near the outer frequency limit.  <i>Reconstructed orthogonal Fourier Plots</i> Reduced $k_z$ -frequency support (corresponding resolution worse than 400 nm).	significantly above 350 nm consider recalibration of the system (requires service engineer).
	Low lateral (xy) resolution	One (or both) 1 <sup>st</sup> order beam is clipped off or lost by TIRF effect (e.g. for longer wavelength and high RI mismatch with culture medium).	<i>Raw Fourier Projection</i> (see above)  <i>Reconstructed Fourier Plots</i> (lateral) Reduced $k_{x,y}$ -frequency support (>150 nm)	[System] Check centering of the beam: remove objective, open the shutter and project beams to a suitable surface in 0.5-1.5 m distance, e.g. a white piece of paper adhered to the ceiling of the incubation chamber. Adjust illumination power as required. Mark the location of each angle's 0 <sup>th</sup> order. (Caution: only to be performed by trained specialist. Do not look directly at laser light!) If significantly off center, the system needs to be realigned (requires service engineer). Zeiss: Use coarser diffraction grids or relay lens with shorter focal length.
<b>1d, S3, S6, S7</b>	Refractive index mismatch artifacts. Intensity side lobes along the z-axis ('ghosting').	Mismatch between the assumed optical response of the system encoded in the OTF, and the effective optical response in the sample region of interest for the specific wavelength and imaging condition.  [Sample] Spherical aberration mismatch either (1) by using immersion medium with wrong refractive index (RI) or operating at wrong temperature, or (2) if sample (region of interest) is far from coverslip or coverslip thickness is wrong, or (3) correction collar of the objective (if equipped with) is set to a wrong position.  [System] Grating position (distance to relay lens) or 'top phase' galvo alignment (OMX Blaze).	<i>Spherical Aberration Mismatch</i> z-minimum variance (ZMV) is relatively high (> 0.5-1, sample-dependent)  One-sided shifted minima relative to mean intensity peak indicate mismatch. <i>Note:</i> check requires suitable sample (flat, well contrasted; e.g. single bead layer). Low z-minimum variance (ZMV) and balanced profile relative to mean intensity profile indicate good match.  [System calibration] <i>Illumination Pattern Focus</i> Record dense 100nm bead layer and test for balanced alignment of the illumination z-	[Sample] Match optical properties of the sample and the OTF.  [Acquisition] Adjust RI of the acquisition immersion oil (or use correction collar) to correct for mismatch induced by imaging depth, sample/medium RI, and temperature.  [System] Ensure temperature stability. Acquire new wavelength-specific OTFs to compensate for long-term system variations. Test the quality of OTFs and matching to system calibration settings by acquiring and reconstructing bead layers.  [System] Run 'Grating Calibration' utility (N-SIM). Adjust grating position or 'top phase' settings (OMX service technician only).



			modulation with the focal plane in all angles.	
<b>1c, S2</b>	Stripes in either 1, 2 or all 3 angles ('hatching'). Reduced structural resolution in affected orientation.	Incorrect angle (k0) used for the reconstruction. Insufficient feature content and/or low modulation contrast does not allow reliable fit.	<i>Reconstructed Fourier Plot</i> Frequency range extends less in the affected orientation(s) => asymmetric 'flower pattern' if 1 or 2 angles are affected.	[Recon] Determine the right k0 values, e.g. from reconstructing dense bead layer or sample with dense, high-contrasted features (OMX: check SIR log file for issued warnings)  If low feature content and contrast does not allow reliable k0 fit, use fixed k0 values (determined from bead layers) – OMX only.
<b>Ref. 15</b>	Stripes in angle direction(s), restricted to very bright regions only.	Oversaturation: Intensity saturated regions in the raw data show no stripes (=> no interference).	<i>Modulation Contrast Map</i> Green color indicates oversaturated pixels in the raw data.	[Acquisition] Reduce excitation light or exposure times to avoid oversaturation or exclude oversaturated areas from consideration/evaluation.
<b>Ref. 15</b>	Stripes, locally confined	Movement of fluorescent particles, features, or cells between acquisition of the different angles, e.g. floating antibody aggregates due to low affinity or poor sample preparation.	<i>Motion &amp; Illumination Variation:</i> Spots/features with distinct cyan, magenta, yellow coloring.	[Sample] Thorough washing, post-fixation with 4% (vol/vol) formaldehyde; use different antibodies or FP-tagged protein. If applicable, exclude affected areas from consideration/evaluation.
	global (unidirectional)	Motion blur of the specimen movement between acquisition of each angle (live cell movements or stage drift)	<i>Motion &amp; Illumination Variation:</i> Coloring of all features with distinct directionality.	[Acquisition] Increase acquisition speed, decrease intervals between angle acquisitions; use OMX Blaze.
	global (multidirectional)	False 'drift correction' setting (OMX).		[Recon] Activate 'drift correction' (OMX with rotary phase grating); deactivate 'drift correction' (OMX Blaze).
<b>S10</b>	Stripes in axial direction (combined with lateral stripes in out-of-focus planes)	Center beam misalignment between angle directions	<i>Reconstructed Fourier Plot - lateral and orthogonal</i> Spots in 3D FFT allow detection of regular stripe pattern in the reconstructed data	[System] Beam realignment necessary (requires service engineer)
<b>1e, S4</b>	6-point hexagonal repeat (or 'honeycomb pattern') can be found globally throughout or at specific, isolated areas of 2D-SIM images, acquired with 2-beam interference (+1, -1)	Spatial, low frequency contribution is missing from axial direction ('missing cone' problem)	<i>Reconstructed Fourier Plot</i> Frequency range is reduced in all directions (symmetrical but shrunken 'flower edges' are observed, as compared to expected resolution).	[Acquisition] Reduce contribution of out-of focus-light via a) TIRF or b) shallow z-stack acquisition. If possible, acquire stack using 3-beam interference (+1, 0, -1) in lieu of 2-beam interference (+1, -1). Reconstruct image using algorithm able to fill in 'missing cone.' (Example: FairSIM, with <i>Attenuation</i> function enabled (ref. 19).
<b>S4</b>	Z-wrapping artifact: Orthogonal coarse stripes and decreased	First/Last frame(s) of a z-stack starts/ends in prominent in-focus sample structure. 3D-	n/a	[Acquisition] Extend height of z-stack, such that the structure of interest are just out of focus in the first and last image planes (i.e. no

	contrast/resolution throughout reconstructed dataset. Prominent echo signals of opposing z-ends.	SIM algorithm 'loops' information from last to first slice to allow the Fourier processing to work as it assumes infinite structures.		stripes visible in the raw image).
<b>5b</b>	Channel misalignment	Chromatic aberration: System instability, tilted emission filter (multi-camera system).	n/a	[Acquisition] Make use of multicolor 3D alignment calibration slide (e.g. 2-layer 200 nm TetraSpeck beads) to determine alignment parameters.

## BOXES

### Box 1 | The SIM principle

The SIM method takes advantage of the addition of high-frequency information to the image when a fluorescent sample is excited with a periodic fine-striped widefield illumination. In the case of the original (2D-)SIM approach<sup>1,2</sup> this pattern consists of lateral stripes of a single frequency, with a stripe distance close to the resolution limit of the optical system (i.e. ~200 nm with a 1.4 NA oil immersion objective). These are generated by the interference of two beams of light, which are positioned to enter the objective's back-focal aperture close to opposite edges (+1/-1 order beams). For the more advanced 3D-SIM approach, the illumination pattern is produced by three beams, the two outer ones near opposite edges of the back aperture plus a central (0 order) beam. This generates illumination containing two lateral frequencies (1<sup>st</sup> and 2<sup>nd</sup> order stripes of ~400 and ~200 nm width, respectively) and in addition an axial modulation near the z-resolution of the optical system, allowing optical sectioning and 2-fold resolution improvement along the optical axis<sup>3</sup>. The structured illumination pattern interacts with the sample, producing a fluorescent image, which contains information at higher spatial frequencies than can usually be observed, corresponding to fine sample details below the diffraction limit. This information is frequency shifted to lower, observable spatial frequencies and mixed with the normally visible lower spatial frequencies, an effect similar to the generation of Moiré fringes. Multiple images are collected with the illumination stripe pattern, laterally shifted to different phase positions (typically 5 steps within the sinusoidal cycle of one wavelength; step size:  $2\pi/5$ ) and rotated (typically in 3 or 5 angles with steps of 60° or 36°, respectively). For the super-resolution reconstruction the data is Fourier transformed to convert it into a spatial frequency representation. The information acquired at different phase positions of the SIM stripes are used as a set of linear equations to separate the relative contributions from the lower frequencies (equivalent to conventional widefield imaging) and higher frequencies (the super-resolution information), a step that is also referred to as 'band separation'. The higher frequencies are extracted and shifted to the correct position in frequency space and different angles are combined to produce a nearly isotropic restoration of the image in the xy-dimension. After reconstruction, a generalized Wiener filter is applied to flatten the frequency response with respect to the OTF and compensate for the different relative contribution of fluorescent information and noise. The data is subsequently scaled to more accurately reflect the contribution at different frequencies, using an expanded OTF (i.e. the OTF of a microscope with twice the resolution; referred to as apodization). Finally, the data is inverse Fourier transformed into real space information, thus producing a resolution-doubled image. Figure panel (a) visualizes these steps for a 3-beam interference illumination, as required for 3D-SIM reconstructions, in spatial and frequency space (example data showing pores in a sub-region of a membrane stained liver endothelial cell<sup>19</sup>).

Importantly, reconstructed super-resolution SIM images not only feature up to 8-fold (3D-SIM) improved volumetric resolution, but also combine this with strong contrast enhancement (in the orders of magnitudes) due to effective rejection of out-of-focus signal, as well as very efficient frequency transfer in the 100-200 nm resolution range<sup>44</sup>. Of note, the reconstruction uses mostly linear processing<sup>3</sup>, and mixes original and shifted frequencies in real space, thus retaining relative intensity differences for subsequent quantitative analyses.

A simulation of the reconstruction process is shown in Figure panel (b) illustrating the generation of high-frequency information. For simplicity only one dimension using a 2-beam interference illumination with three phase steps is shown with the y-axis representing arbitrary intensity units, and the x-axis representing physical space in nm. For each setting of the illumination pattern phase (dotted grey line in the lower three diagrams), different areas of the '1D sample' containing two bright and two less bright emitters (grey bars, 20 nm wide) are excited, which generate three different signal responses (red, green and blue curves, respectively, fitted to 40 nm pixel intensities represented by thinner angular lines underneath). Using this extra information, close-by 'fluorophores' (two grey bars on the left side), indistinguishable in widefield can be separated after the SIM reconstruction (upper panel, cyan

and magenta curves, respectively). The contrast between emitters that are just resolvable in widefield (two grey bars on the right, spaced close to the resolution limit) also improves, while relative signal intensity differences between single emitters are preserved.

Importantly, recombining the different spatial frequency components requires good knowledge of the amplitude at which the optical system transfers this information. This is usually extracted from the system's OTF. Only when the system's OTF and the sample properties during acquisition are reasonably matched, will the reconstruction algorithm produce valid results, virtually free from notable artifacts. Irregularities, such as spherical aberration, significantly affect the amplitude of information transfer with spatial frequency, and hence the quality of reconstructions, as the computational algorithm can no longer properly match the intensity of different components during processing.

Another critical factor is the amplitude of the stripe modulation in the collected images. The stripes enable the shifting of uncollectable high spatial frequency information to lower collectable frequencies. The contrast of these stripes is directly linked to the amount of the retrievable high-frequency information. Figure panel (c) illustrates a simulation of SIM reconstructions at different modulation depth and background levels (indicated by solid gray line). High modulation and high sample SNR with low background yields a high-quality reconstruction (c, left; high contrasted separation of the two emitters, linear relationship of their intensities). For high modulation depth, but low sample SNR (e.g. by increased out-of-focus background), additional shot noise enters the reconstruction and degrades image quality (c, middle). For high sample SNR, but low SIM pattern contrast, the resolution improvement becomes hardly noticeable (c, right). By using the *modulation contrast / modulation contrast map* functions in *SIMcheck*, the stripe modulation can be measured and mapped to the reconstructed data enabling assessment of regions where SIM has worked well and where it has not.

In the extreme case of no stripe contrast the image is simply a conventional (diffraction limited) widefield image that, dependent on the Wiener filter setting, is more or less interwoven with the characteristic 'hammerstroke' pseudo-structure from reconstructing unmodulated noise (shown in **Figs. 1b, 2** and **Supplementary Fig. 1**). Increasing the Wiener filter constant reduces reconstructed noise artifacts, albeit at the expense of blurring the reconstructed image and thereby (seemingly) reducing its resolution. However, in raw SIM data with lowered modulation contrast, high-resolution information is less present in the first place and therefore increasing the Wiener filter generates a more realistic representation of the 'effective' achievable resolution. Furthermore, Wiener filtering should be applied sparingly, as over-filtering generates other characteristic artifacts (visible as cartwheel shaped Fourier plot). Importantly, no filtering can ever compensate for low SNR/modulation contrast in the input data, and can only reduce detrimental effects to a small extent.

Finally, the resolution improvement achieved in SIM relies on both a fine spacing and a high modulation depth of the excitation light pattern. Therefore, a coherent light source (i.e., a laser) capable of introducing destructive interference in the pattern is required for maximum contrast and thus best performance. Incoherent light sources (such as LEDs) can only be used when compromises in resolution improvement or SNR are acceptable.

## **Box 2 | Publishing guidelines**

SIM is a highly complex method, and the increasing prominence of SIM data in biological publications - especially when it is included as one minor component of a larger study - poses a significant problem due to the relative lack of experience of many users and manuscript reviewers. The requirement for (1) complex data processing using proprietary software, and (2) user-acquired, system specific calibration files (e.g. OTFs) adds to this burden. With this in mind we suggest a series of steps to ensure that data submitted, and eventually accepted for publication, is of adequate quality to justify deduced conclusions.

1. Representative raw and reconstructed data displaying the full 32- or 16-bit range (as

- appropriate) should be included as supplements or made otherwise available.
2. Raw data for the entire publication should be in a single, verifiable location, ideally a structured database such as OMERO<sup>45</sup>, easily producible upon request. These data should include not only raw image sets but also any associated calibration files, such as OTFs and image registration standards, otherwise repeat processing will be impossible.
  3. Discarding negative values in the reconstruction process (sometimes a default option in commercial software packages) must be avoided. Reconstructed data prior to image analysis or presentation should comprise the full dynamic range.
  4. For main figures, thresholding of intensity values below 0, or the modal value, is acceptable, but should be noted in Supplementary Methods. When data contains significant contribution from label-free background, it is preferred to threshold intensity values to the mode value, rather than to 0, as reconstruction noise centers around the mode, while 0 may be variable in relation to the noise center between datasets.
  5. Maximum intensity projections must be clearly indicated as such.
  6. Line profile plots of the unmodified reconstructed data through the structure of interest and neighboring background areas are recommended.
  7. For multi-channel studies, details of channel alignment (reference sample, software used, any other corrections) must be included in the (Supplementary) Methods section.
  8. Highly structured, iterative patterns (hexagons, triangles, repeated lines, etc.) must be highly scrutinized before being identified as biological structures, as many reconstruction artifacts have a similar appearance (regular polygons with angles equal to stripe rotations).
  9. High-frequency noise filter settings (Wiener or other) used in the reconstruction software should be indicated in (Supplementary) Methods.
  10. The approach for OTF generation (user- or system-generated), and whether and how this is matched to the sample PSF should be indicated in the (Supplementary) Methods.
  11. The functional resolution (lateral and axial) of the system used should be assessed empirically through calculation of either full-width half-maximum of diffraction-limited structures or beads<sup>28</sup>, radial Fourier plots of reconstructed data<sup>13</sup>, or Fourier ring correlation (FRC)-based methods<sup>46</sup>. The achieved resolution, rather than the theoretical resolution, should then be considered in the study before drawing biologically relevant conclusions.
  12. Essential details on system configuration (if accessible):
    - System (make/model, any modifications)
    - Objectives (make, magnification, numerical aperture, correction, etc.)
    - Laser lines (wavelength); potentially power, source, coupling (for bespoke systems)
    - Dichroic and emission filter sets.
    - Camera settings/parameters (type, make/model, bit depth, etc.)
    - Method (2D-SIM, 3D-SIM, TIRF-SIM, etc.)
    - Acquisition modality (number of angles, number of phases, pixel size, z-step size, etc.)
  13. A general range of acquisition parameters (laser power, exposure time, etc.) and reconstruction parameters (background offset, changes in default settings of apodization, filtering, or other parameters) should be included.
  14. Quantification of signal distributions or proximity should accompany representative images.
  15. Technical replicates of at least n=10 (e.g. cells on the same slide), and biological replicates of at least n=2, are recommended for qualitative or illustrative data. Technical replicates of at least 10 and biological replicates of at least 3 are recommended for quantitative studies.
  16. Perform a 'reality check'. Are the biological conclusions (such as physical distances between protein factors) within the resolution range permitted by the system? Are any changes in distributions between targets affected by the channel alignment parameters? Can any unique or interesting patterns be explained by documented SIM artifacts before being attributed as a biological phenomenon?

## REFERENCES

1. Heintzmann, R. & Cremer, C. G. Laterally modulated excitation microscopy: improvement of resolution by using a diffraction grating. *Proc. SPIE* **3568**, 185–196 (1999).
2. Gustafsson, M. G. L. Surpassing the lateral resolution limit by a factor of two using structured illumination microscopy. *J Microsc* **198**, 82–87 (2000).
3. Gustafsson, M. G. L. *et al.* Three-dimensional resolution doubling in wide-field fluorescence microscopy by structured illumination. *Biophys J* **94**, 4957–4970 (2008).
4. Schermelleh, L. *et al.* Subdiffraction multicolor imaging of the nuclear periphery with 3D structured illumination microscopy. *Science* **320**, 1332–1336 (2008).
5. Sahl, S. J. *et al.* Comment on ‘Extended-resolution structured illumination imaging of endocytic and cytoskeletal dynamics’. *Science* **352**, 527–527 (2016).
6. Li, D. & Betzig, E. Response to Comment on ‘Extended-resolution structured illumination imaging of endocytic and cytoskeletal dynamics’. *Science* **352**, 527–527 (2016).
7. Shao, L. & Rego, E. H. in *Fluorescence Microscopy* 213–225 (Elsevier, 2014).
8. Allen, J. R., Ross, S. T. & Davidson, M. W. Structured Illumination Microscopy for Superresolution. *ChemPhysChem* **15**, 566–576 (2014).
9. Rego, E. H. & Shao, L. Practical structured illumination microscopy. *Methods Mol Biol* **1251**, 175–192 (2015).
10. Fiolka, R. in *Quantitative Imaging in Cell Biology* **123**, 295–313 (Elsevier, 2014).
11. Komis, G. *et al.* Superresolution live imaging of plant cells using structured illumination microscopy. *Nat Protoc* **10**, 1248–1263 (2015).
12. Engel, U. in *Quantitative Imaging in Cell Biology* **123**, 315–333 (Elsevier, 2014).
13. Ball, G. *et al.* SIMcheck: a Toolbox for Successful Super-resolution Structured Illumination Microscopy. *Sci. Rep.* **5**, 15915 (2015).
14. Terui, Y. Image processing for structured illumination microscopy. in 1–3 (IEEE, 2015).
15. Kraus, F. *et al.* Quantitative 3D structured illumination microscopy of nuclear structures. *Nat Protoc*
16. Young, L. J., Ströhl, F. & Kaminski, C. F. A Guide to Structured Illumination TIRF Microscopy at High Speed with Multiple Colors. *J Vis Exp* (2016).
17. Turnbull, L. *et al.* Super-resolution Imaging of the Cytokinetic Z Ring in Live Bacteria Using Fast 3D-Structured Illumination Microscopy (f3D-SIM). *J Vis Exp* e51469–e51469 (2014).
18. Křížek, P., Lukeš, T., Ovesný, M., Fliegel, K. & Hagen, G. M. SIMToolbox: a MATLAB toolbox for structured illumination fluorescence microscopy. *Bioinformatics* **btv576** (2015).
19. Müller, M., Mönkemöller, V., Hennig, S., Hübner, W. & Huser, T. Open-source image reconstruction of super-resolution structured illumination microscopy data in ImageJ. *Nat Commun* **7**, 10980 (2016).
20. Gustafsson, M. G. L. Nonlinear structured-illumination microscopy: Wide-field fluorescence imaging with theoretically unlimited resolution. *Proceedings of the National Academy of Sciences* **102**, 13081–13086 (2005).
21. Rego, E. H. *et al.* Nonlinear structured-illumination microscopy with a photoswitchable protein reveals cellular structures at 50-nm resolution. *Proc Natl Acad Sci USA* **109**, E135 (2012).
22. Li, D. *et al.* Extended-resolution structured illumination imaging of endocytic and cytoskeletal dynamics. *Science* **349**, aab3500–aab3500 (2015).
23. Eggeling, C. & Hell, S. W. in *Far-Field Optical Nanoscopy* 3–26. (Springer, 2014).
24. Müller, T., Schumann, C. & Kraegeloh, A. STED microscopy and its applications: new insights into cellular processes on the nanoscale. *ChemPhysChem* **13**, 1986–2000 (2012).

25. Shao, L., Kner, P., Rego, E. H. & Gustafsson, M. G. L. Super-resolution 3D microscopy of live whole cells using structured illumination. *Nat Methods* **8**, 1044–1046 (2011). Shao, L., Kner, P., Rego, E. H. & Gustafsson, M. G. L. Super-resolution 3D microscopy of live whole cells using structured illumination. *Nat Methods* **8**, 1044–1046 (2011).
26. Betzig, E. *et al.* Imaging intracellular fluorescent proteins at nanometer resolution. *Science* **313**, 1642–1645 (2006).
27. Liu, Z., Lavis, L. D. & Betzig, E. Imaging Live-Cell Dynamics and Structure at the Single-Molecule Level. *Mol Cell* **58**, 644–659 (2015).
28. Wegel, E. *et al.* Imaging cellular structures in super-resolution with SIM, STED and Localisation Microscopy: A practical comparison. *Sci. Rep.* **6**, 27290 (2016).
29. Fiolka, R., Shao, L., Rego, H. E., Davidson, M. W. & Gustafsson, M. G. L. Time-lapse two-color 3D imaging of live cells with doubled resolution using structured illumination. *Proc Natl Acad Sci USA* **109**, 5311 (2012).
30. Rothbauer, U. *et al.* Targeting and tracing antigens in live cells with fluorescent nanobodies. *Nat Methods* **3**, 887–889 (2006).
31. Grimm, J. B. *et al.* A general method to improve fluorophores for live-cell and single-molecule microscopy. *Nat Methods* **12**, 244–250 (2015).
32. Olivier, N., Keller, D., Rajan, V. S., Gönczy, P. & Manley, S. Simple buffers for 3D STORM microscopy. *Biomed. Opt. Express*, *BOE* **4**, 885–899 (2013).
33. MacDonald, L., Baldini, G. & Storrie, B. Does Super-Resolution Fluorescence Microscopy Obsolete Previous Microscopic Approaches to Protein Co-localization? *Methods Mol Biol* **1270**, 255–275 (2015).
34. Cerase, A. *et al.* Spatial separation of Xist RNA and polycomb proteins revealed by superresolution microscopy. *Proceedings of the National Academy of Sciences* **111**, 2235–2240 (2014).
35. Schmied, J. J. *et al.* DNA origami-based standards for quantitative fluorescence microscopy. *Nat Protoc* **9**, 1367–1391 (2014).
36. Marno, K. *et al.* The evolution of structured illumination microscopy in studies of HIV. *Methods* **88**, 20–27 (2015).
37. Schaefer, L. H., Schuster, D. & Schaffer, J. Structured illumination microscopy: artefact analysis and reduction utilizing a parameter optimization approach. *J Microsc* **216**, 165–174 (2004).
38. Shroff, S., Fienup, J. & Williams, D. OTF compensation in structured illumination superresolution images. *Proceedings of SPIE* **7094**, (2008).
39. Débarre, D., Botcherby, E. J., Booth, M. J. & Wilson, T. Adaptive optics for structured illumination microscopy. *Opt Express* **16**, 9290–9305 (2008).
40. Righolt, C. H. *et al.* Image filtering in structured illumination microscopy using the Lukosz bound. *Opt Express* **21**, 24431 (2013).
41. Wicker, K., Mandula, O., Best, G., Fiolka, R. & Heintzmann, R. Phase optimisation for structured illumination microscopy. *Opt Express* **21**, 2032–2049 (2013).
42. Schindelin, J. *et al.* Fiji: an open-source platform for biological-image analysis. *Nat Methods* **9**, 676–682 (2012).
43. Schneider, C. A., Rasband, W. S. & Eliceiri, K. W. NIH Image to ImageJ: 25 years of image analysis. *Nat Methods* **9**, 671–675 (2012).
44. Demmerle, J., Wegel, E., Schermelleh, L. & Dobbie, I. M. Assessing resolution in super-resolution imaging. *Methods* **88**, 3–10 (2015).
45. Allan, C. *et al.* OMERO: flexible, model-driven data management for experimental biology. *Nat Methods* **9**, 245–253 (2012).
46. Nieuwenhuizen, R. P. J. *et al.* Measuring image resolution in optical nanoscopy. *Nat Methods* **10**, 557–562 (2013).
47. O'Holleran, K. & Shaw, M. Optimized approaches for optical sectioning and resolution enhancement in 2d structured illumination microscopy. *Biomed Optics Exp*, **5**, 2580–2590 (2014).

## FIGURE LEGENDS

**Figure 1** | Biological showcase of commonly presented SIM reconstruction artifacts. **(a)** Maximum z-projection of a mouse C127 epithelial cells immunostained for tubulin (Alexa Fluor 488), and counterstained with DAPI exemplifying typical SIM reconstruction artifacts. The blue box denotes the region shown in panel **b**, the blue arrowhead denotes the position of the orthogonal view in panel **c**, and the green box denotes the region shown in panel **d**. **(b)** Optical section of the DAPI stained nucleus depicted in panel **a**. Insets expanded to emphasize high-frequency noise contribution, as represented by 'hammerstroke' artifacts, in a background region (small inset) or superimposing genuine features of labeled chromatin (large inset). **(c)** Orthogonal view demonstrating aberration by a 'lensing' effect caused by a refractive index mismatch between the stained nucleus and the surrounding (arrowheads). **(d)** Detail view of tubulin staining depicted in panel **a**, when reconstructed with incorrect angle ( $k_0$ ) settings, leading to 'hatching' of angle-specific stripes intermixed with the genuine tubulin signal. **(d')** Same region reconstructed with correct angle settings showing no hatching artifact. **(e)** SIM reconstruction of an MDCK cell immunostained for tubulin (Alexa Fluor 488) and desmoplakin C-terminus (Alexa Fluor 568) imaged using immersion oil whose refractive index is too low for the sample **(e)**. Desmoplakin channel only is shown (right) to emphasize the 'ghosting' artifact of structures displaying multiple echo signals along the optical axis (arrows in the orthogonal view). **(e')** In contrast, when imaged with optimally matched oil, tubulin signals appear sharper (compare insets in lateral views), and only a single layer of desmoplakin signal is seen. **(f)** U2OS cell stained with Phalloidin-ATTO488 for actin and imaged with 2D-SIM, showing 'honeycomb' artifacts as consequence of out-of-focus blur contribution to the reconstruction (left, inset). **(f')** Artifacts are reduced by OTF attenuation in the *fairSIM* reconstruction algorithm (right), which rejects the contribution from out-of-focus signal<sup>47</sup>. Reconstructed images in all panels are shown after thresholding to discard negative intensity values (clipping/baseline subtraction). Bars: 5  $\mu\text{m}$  and 1  $\mu\text{m}$  (insets).

**Figure 2** | Identifying differences in modulation contrast. DAPI-stained C127 cells with either low modulation contrast **(a)** or high modulation contrast **(g)**, and the resulting diagnostic readouts (upper two rows and bottom two rows) from *SIMcheck*. The left most column shows representative raw data **(a)** and **(g)** with intensity minima, maxima, and camera type (top), and insets below **(a')** and **(g')** showing near absence or presence of structured illumination pattern imposed on the sample's signal. The second column shows raw data checks: **(b)** and **(h)** modulation contrast to noise (MCN) output from *SIMcheck* of a single frame of the image stack, with each pixel assigned a heatmap value, and the average modulation contrast to noise ratio (MCNR) value for the image noted in the bottom left corner; **(c)** and **(i)** Maximum intensity projection of the FFT of the raw data (FPJ output from *SIMcheck*), showing less extended cloud of high-frequency information and slightly weaker second-order spots from the low modulation contrast data. Third column: Lateral **(d)** and **(j)** and orthogonal **(d')** and **(j')** views of the reconstructed images superimposed with the MCN map shown previously (MCM), illustrating the difference in reconstruction output as a function of modulation contrast in the raw image. Boxed insets show detail of chromatin. Purple and dark red features highlight reconstructed pseudo-structures with low underlying modulation contrast, which are not considered trustworthy. Fourth column: Non-thresholded lateral **(e)** and **(k)** and orthogonal **(e')** and **(k')** views of the reconstructed image. In **e** and **e'** reconstruction results for using low and high Wiener filter settings are displayed side by side separated by dashed diagonal line. Corresponding intensity histograms of reconstructed stacks, with respective intensity minima, maxima, modes and the minimum-to-maximum ration (MMR) are displayed as insets. Values of assigned floating-point data are displayed as log-scale (grey) and linear-scale (black) histograms from the 'Reconstructed Intensity Histogram' (RIH) output of *SIMcheck*. Fifth column: **(f)** and **(l)** Reciprocal-space images of log-scaled 3D FFT of reconstructed data, with correlated dimensions in real space superimposed as rings and denoted in  $\mu\text{m}$ ; **(f')** and **(l')** Corresponding radial profile of amplitude component from the 3D FFT of reconstructed data 'Fourier Transform Radial (FTR)' output from *SIMcheck*. Amplitude is indicated in arbitrary units on the y-axis, and



reciprocal distance on the x-axis, denoted in either  $\mu\text{m}^{-1}$  or non-reciprocally in nm (*italics*). Note the difference in shape of in the FTR plots between low modulation contrast data (with either low or high Wiener filter setting), and high modulation contrast data. Generally, a flat central profile together with steep drops at the center and towards the edge of the theoretical frequency/resolution limit (indicated by blue dashed circle and line in the FTL and FTR at  $\sim 100$  nm and  $\sim 110$  nm, respectively) is indicative of a poor reconstruction, whereas a more straight-line decline is indicative for high data quality. Note also that the relative quality difference correlates with both MMR and MCNR values. Bars:  $5\ \mu\text{m}$  and  $1\ \mu\text{m}$  (insets).

**Figure 3** | Overview of the workflow for SIM experiments. **(a)** Workflow of the holistic SIM imaging process. Areas covered in this protocol are included in solid boxes, while areas covered in Ball et al.<sup>13</sup> and Kraus et al.<sup>15</sup> are included in dashed boxes. Central aims of the workflow are highlighted in the purple circle, and key points for the user to affect the imaging result are listed in the purple rectangle. Locations in the workflow where *SIMcheck* can be utilized are illustrated. More detailed checklists are provided in **Supplementary Fig. 5** and in the **Supplementary Manual**. **(b)** Schematic of procedure for assembling calibration slides and acquiring calibration datasets.

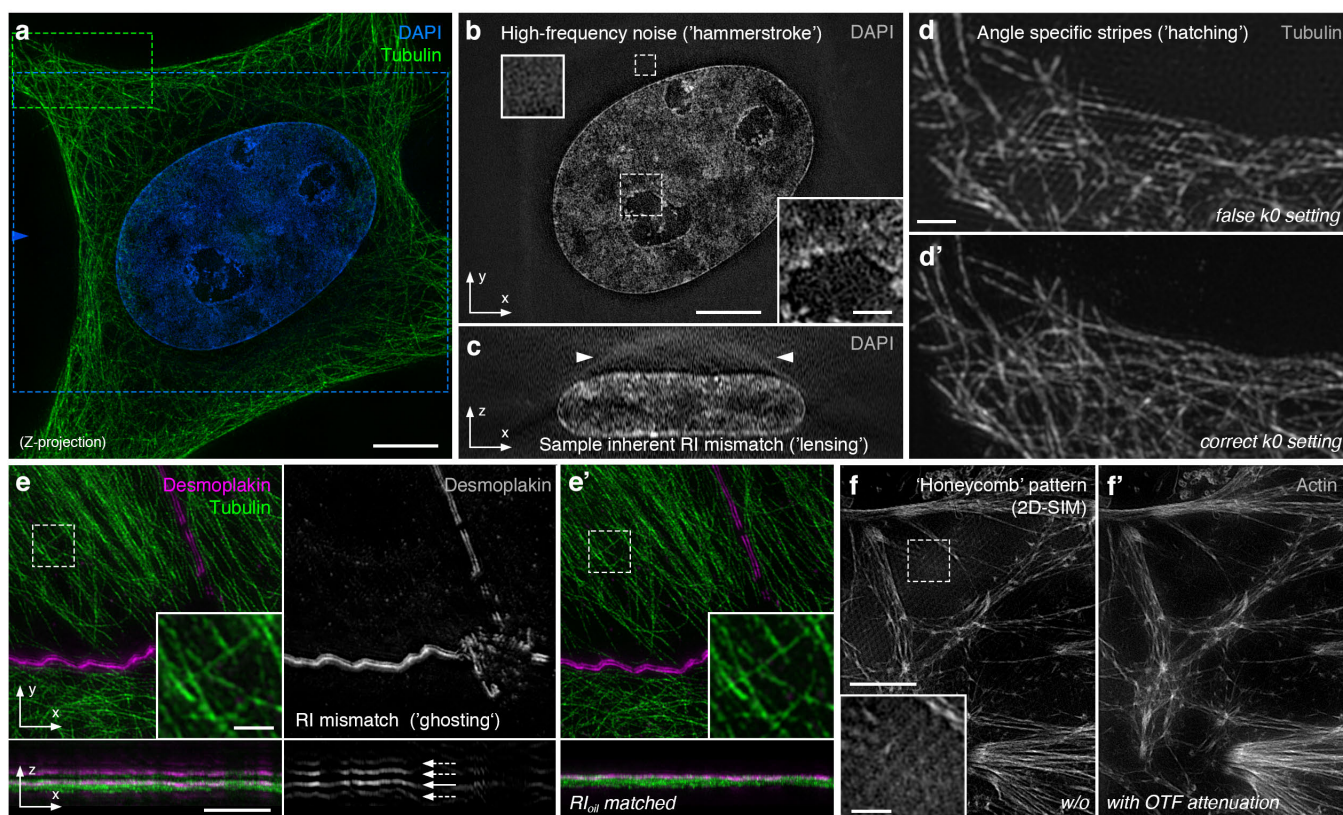
**Figure 4** | Preparation of calibration bead slide set. An overview presenting the initial set-up required prior to biological sample imaging showing required materials and slide assembly steps, as explained in detail in the Procedure section of the protocol.

**Figure 5** | Expected outcomes from calibration slide preparation. **(a)** PSF slides should provide well distributed single beads attached to the coverslip surface to be recorded individually in a  $256 \times 256$  pixel frame, as shown here in widefield mode. The orthogonal view of the bead is below, with axial depth indicated in  $\mu\text{m}$  on the x-axis. The inset is displayed at the same scale, but with a gamma correction to illustrate the symmetry of the PSF and absence of any artifact. **(b)** Expected outcome of 3D multicolor alignment slide, with a 200-nm diameter TetraSpeck bead field shown before (left top panel) and after (right top panel) alignment with image registration software. The orthogonal views of each result are shown below. Note the axial separation of both layers along the z-axis, and the typical degree of channel separation illustrated in the top inset. **(c)** Outcomes from 100-nm-bead layer slides (green emitting beads shown in SI and widefield). Bead fields should neither have too sparse patches of beads (left), nor should beads form very dense multilayers stacked on top of each other (middle). Ideal are intermediate sized patches of bead monolayer interspersed by bead-free background areas (right panel). **(d)** Top panels show a bead-field collected with reduced stripe contrast due to misalignment of the axial interference pattern; bottom panels show the correctly aligned axial interference pattern leading to improved stripe contrast. Leftmost panels: representative single frame from raw data, with structured illumination pattern highlighted in inset, and arrowhead pointing to a typical instance of the pattern. Central panels: *SIMcheck* 'Illumination Pattern Focus' (IPF) module output, showing the orthogonal projection of re-sliced raw data in which the axial interference pattern is visible in the bead layer, for each illumination angle (A1 through A3). Rightmost panels: inset from box in central panels showing a sub-optimal 'zipper' pattern in the axial interference (top), and the desired pattern of axial interference (bottom), corresponding to the relative contrast of stripes as seen in the inset of the leftmost panels. **(e)** Expected outcomes from bead-layer slides with combinations of sub-optimal axial interference pattern (z-illumination) and sub-optimal OTFs (collected with unmatched immersion medium RI). The rightmost panel has both compromised z-illumination and incorrect OTF matching, and shows a low MMR value and a high ZMV value (see **Fig. 2**), with a pronounced intensity dip below the bead field (arrow). The center panel has optimized z-illumination, but incorrect OTF matching, showing a higher MMR value and lower ZMV value. The right panel has optimized z-illumination and correct OTF matching, showing the highest MMR value and the lowest ZMV value, along with a total reduction of intensity dips around the bead field. All bars:  $5\ \mu\text{m}$  and  $1\ \mu\text{m}$  (insets).

**Figure 6** | Matching OTFs and experimental conditions in the sample for multicolor acquisitions. (a) Schematic representation of PSFs as a function of wavelength, depth and immersion oil RI ( $n_{oil}$ ). Left panel: for the three displayed wavelengths, at a given reference value of the immersion oil RI, the PSF (shown as hourglasses) will be horizontally symmetrical. If green is the reference channel, then the optimal RI for 405 nm will be 0.001 units reduced from the reference and the optimal RI for 592 nm will be 0.003 increased from the reference (e.g. 1.511 for 405 nm and 1.515 for 592 nm, with a 488 reference RI of 1.512). Right panel: during image acquisition using the green reference oil (e.g. 1.512), the point-spread behavior within the sample on the coverslip level will deviate (illustrated by the relative PSF shape). The blue PSF will become slightly asymmetric towards the coverslip (bottom-heavy), while the red PSF will become significantly top-heavy (the degree of asymmetry is indicated as the difference between the RI of the oil used and the channel specific optimum RI, e.g.  $1.512 - 1.515 = -0.003$ ; hence it is given the index -3). Using a higher immersion oil RI optimal for the red channel would match the PSF for the red channel for signals on the coverslip level, but at the same time shift the optimum for blue and green deeper into the sample. Accordingly the 'safe z-range' around the optimum (indicated by the vertical bars, narrowing with longer wavelengths) wherein SIM can be performed at minimal risk of spherical aberration artifacts, will be shifted. (b) Left panel: schematic of differences in PSFs of different wavelengths collected at the indicated immersion medium RIs, showing that OTFs collected at a given RI will always contain bias towards one channel or another – optimizing for any one channel brings a trade-off in other spectral ranges. Right panel: the effect of adapting the acquisition conditions of the OTF (boxed PSFs), on PSFs in the sample. Introducing an OTF set acquired with the same RI oil (either optimized for blue/green or red) unifies the 'safe zone' for a given set of wavelengths. These point-spread characteristics for all given channels can be adapted to the depth of interest by increasing the RI of the oil used for the acquisition (e.g. by approx.  $4\ \mu\text{m}$  per 0.002 RI increase). (c) Workflow for selecting immersion medium RI for both acquisition and OTF creation. On the left is a workflow diagram for determining the optimal immersion oil. Starting with the reference of a RI that gives a symmetrical PSF for 488 nm beads on the coverslip, add or subtract the indicated RI for each subsequent choice, until arriving at the final RI for acquisition. This includes accommodations for the mounting medium, which channel the OTF should be optimized for, the optimal depth of the target structure, and any changes in temperature. With a reference RI of 1.512, following the solid black lines will give a result of an acquisition RI of 1.516, while following the dotted line, with a different set of experimental criteria, will also give a value of 1.516 but for a different set of reasons. Other possible combinations are indicated in grey lines. Of note, the numbers and references given are empirically determined on a GE OMX V3 Blaze system, and may differ between manufacturers or among individual systems.

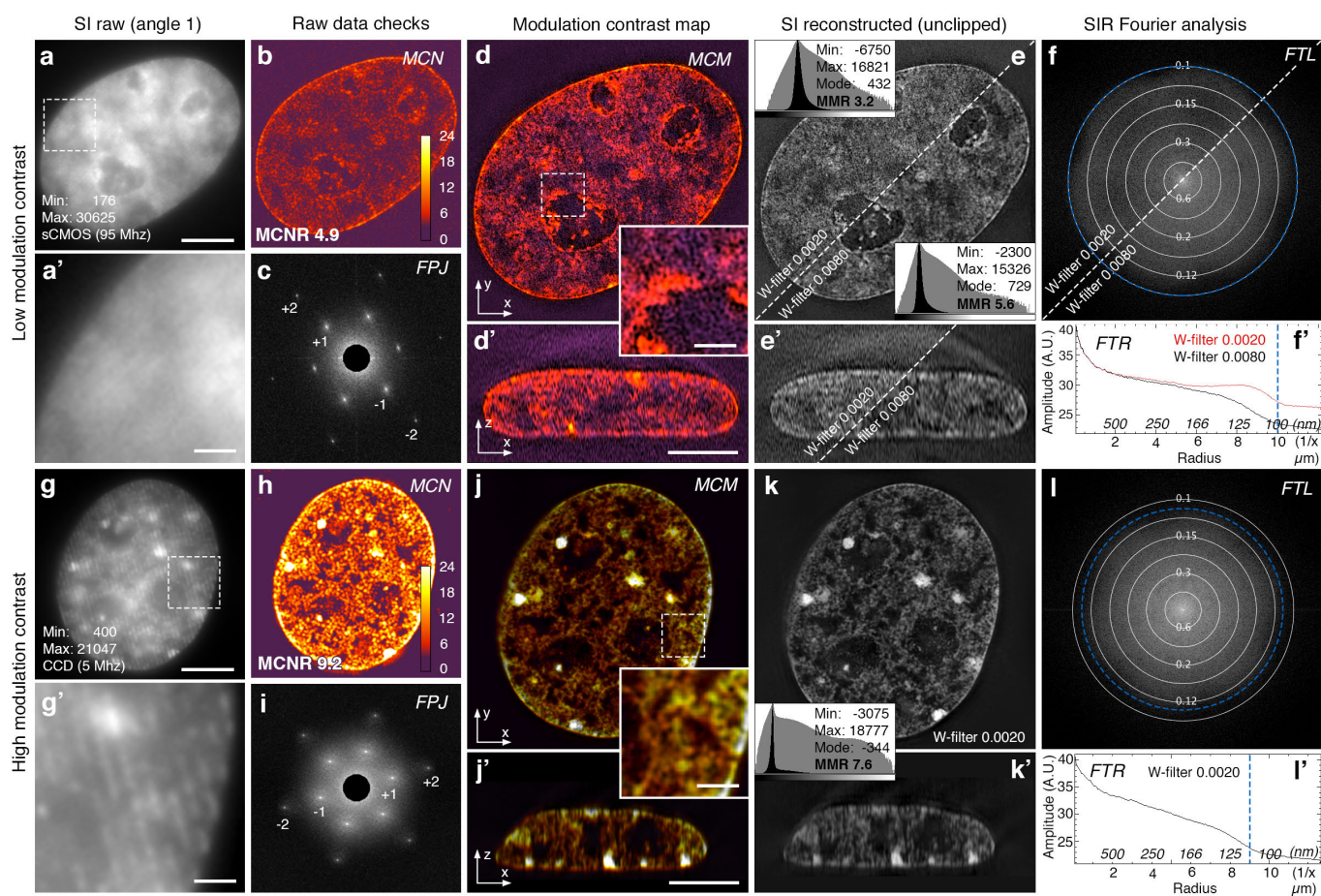
# FIGURES

Figure 1





**Figure 2**



**Figure 3**

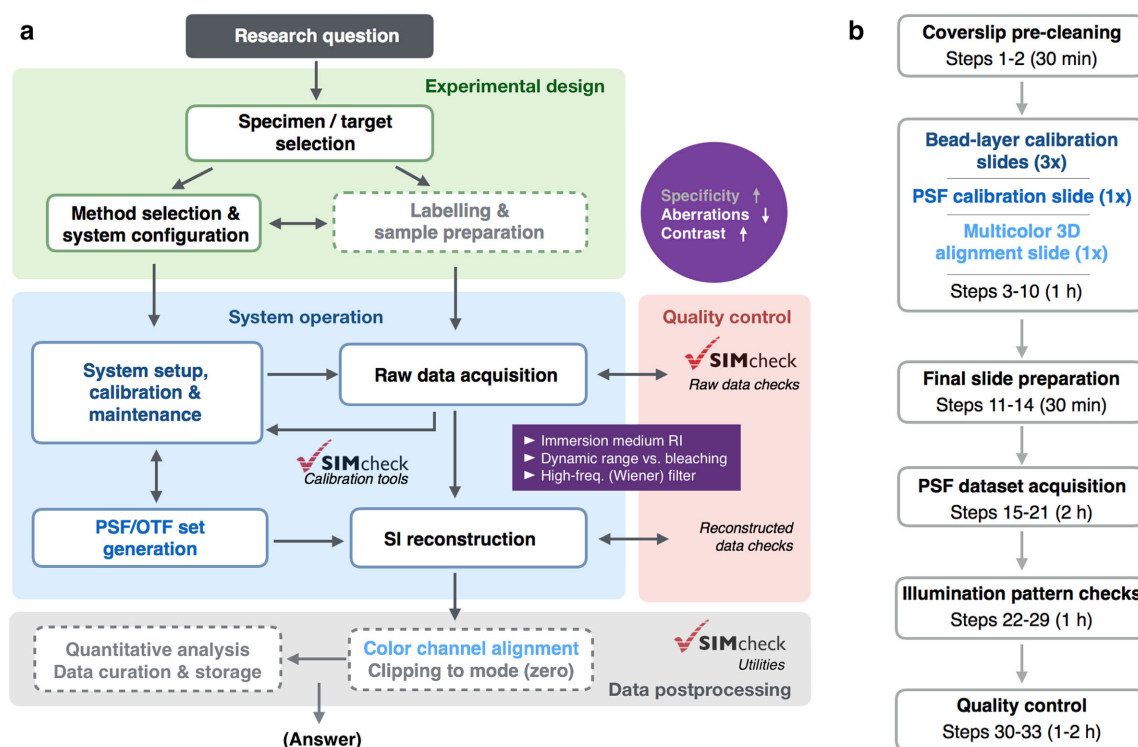


**Figure 4**

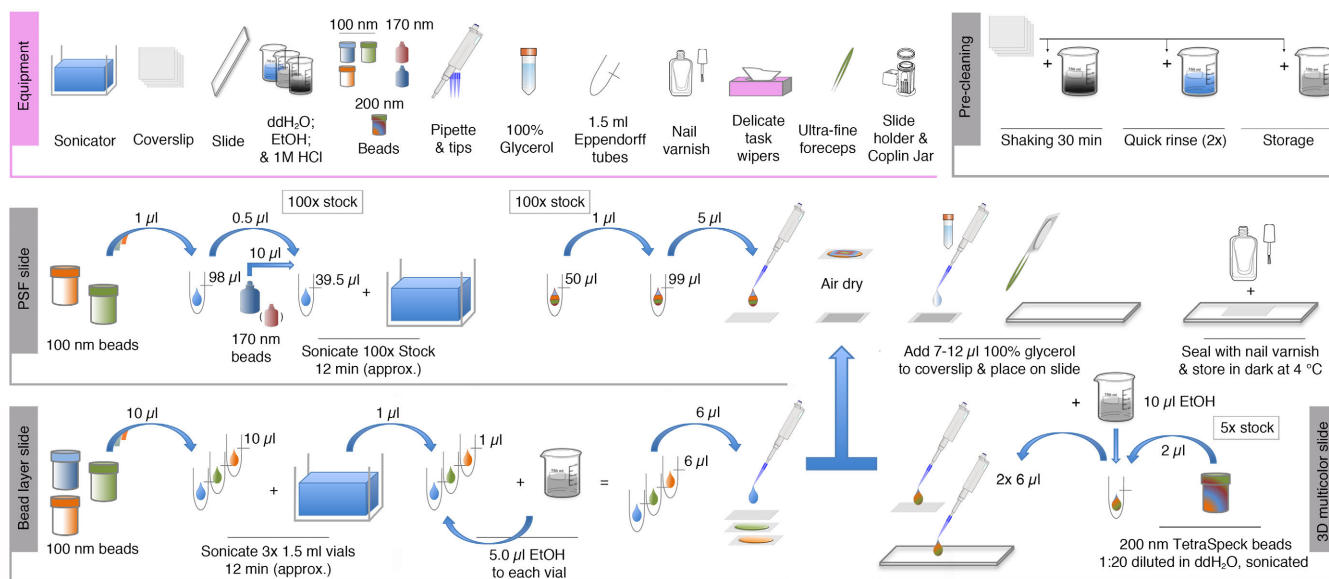


**Figure 5**

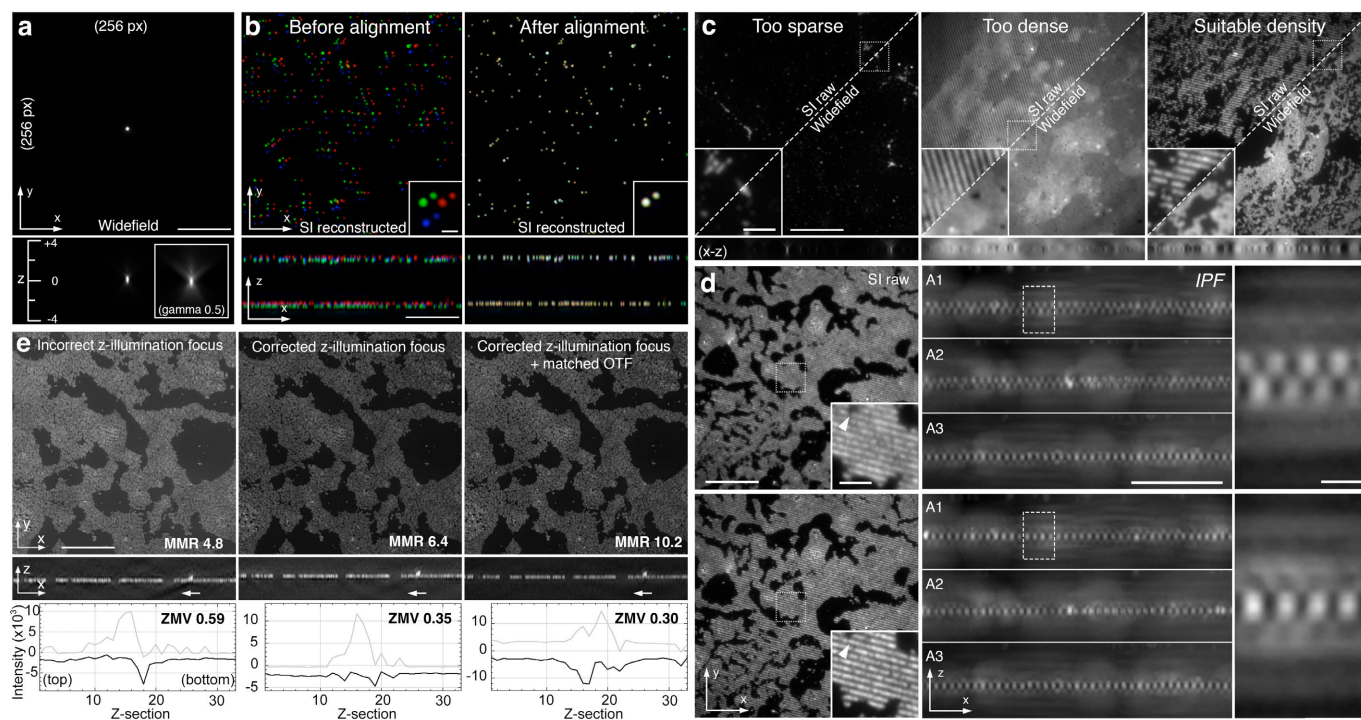


**Figure 6**

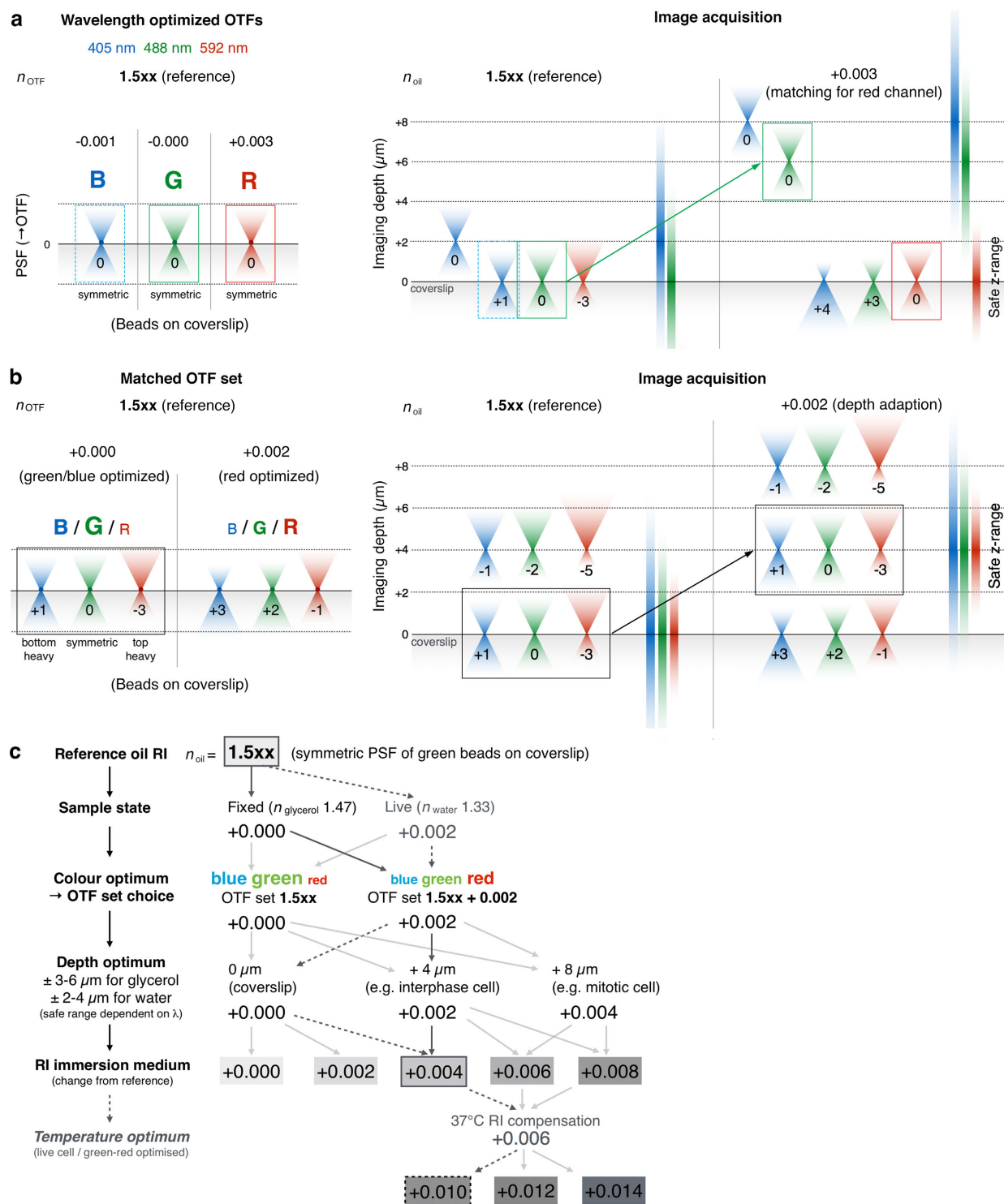
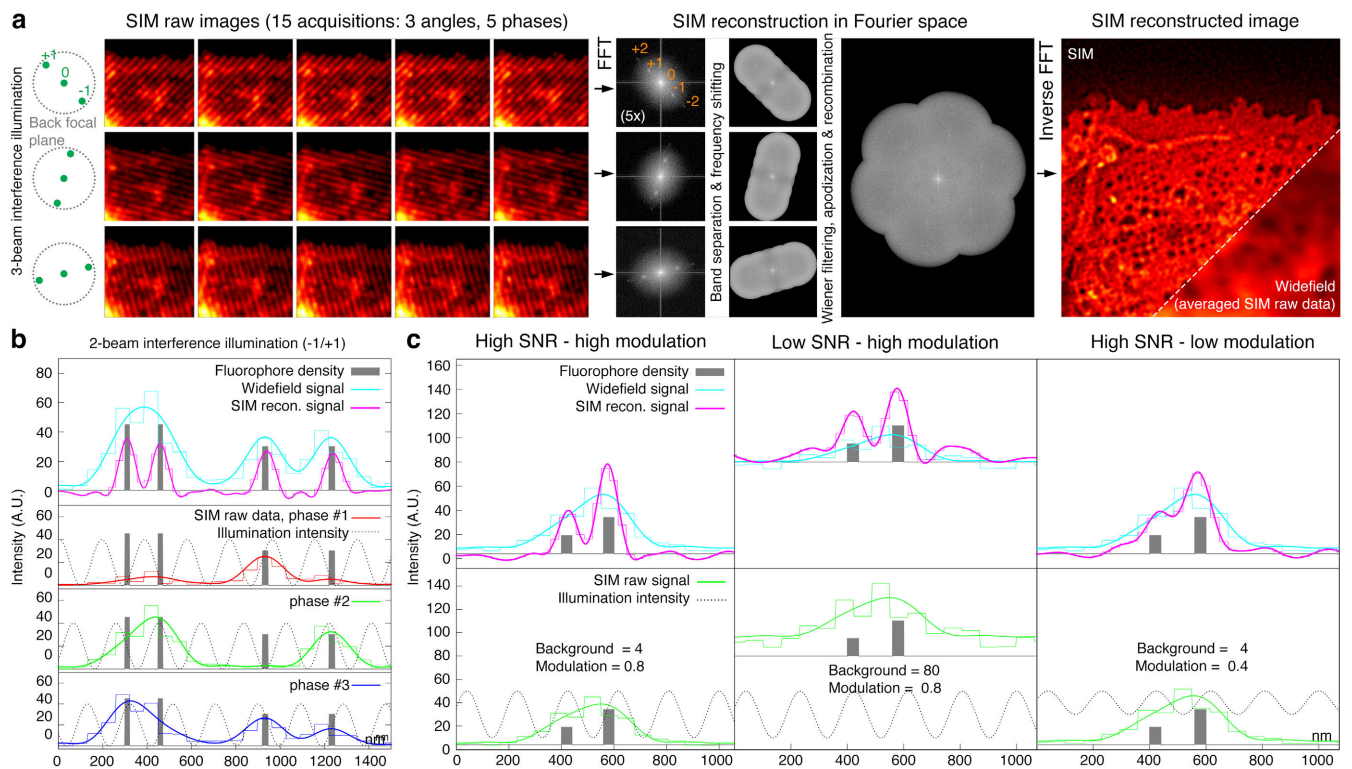




**Figure Box 1**



## **SUPPLEMENTARY INFORMATION**

### **Strategy and tactics for successful structured illumination microscopy**

Justin Demmerle<sup>1,8</sup>, Cassandravictoria Innocent<sup>1,8</sup>, Alison J. North<sup>2</sup>, Graeme Ball<sup>1,3</sup>, Marcel Müller<sup>4</sup>, Ezequiel Miron<sup>1</sup>, Atsushi Matsuda<sup>5,6</sup>, Ian M. Dobbie<sup>1</sup>, Yolanda Markaki<sup>7</sup>, Lothar Schermelleh<sup>1</sup>

<sup>1</sup>Micron Advanced Bioimaging Unit, Department of Biochemistry, University of Oxford, Oxford OX1 3QU, UK

<sup>2</sup>Bio-Imaging Resource Center, The Rockefeller University, New York, NY 10065, USA.

<sup>3</sup>Current Address: Dundee Imaging Facility, School of Life Sciences, University of Dundee, Dundee, DD1 5EH, UK.

<sup>4</sup>Biomolecular Photonics Group, Faculty of Physics, Bielefeld University, Universitaetsstrasse 25, 33615 Bielefeld, Germany.

<sup>5</sup>Advanced ICT Research Institute Kobe, National Institute of Information and Communications Technology, Kobe 651-2492, Japan

<sup>6</sup>Graduate School of Frontier Biosciences, Osaka University, Osaka 565-0871, Japan

<sup>7</sup>David Geffen School of Medicine, Department of Biological Chemistry, UCLA, Los Angeles, CA 90095, USA

<sup>8</sup>These authors contributed equally to this work.

Correspondence should be addressed to L.S. (lothar.schermelleh@bioch.ox.ac.uk).

**Supplementary Manual**  
**Supplementary Table**  
**Supplementary Protocol**  
**Supplementary Figures 1-10**



## A Experimental design



### Specimen / target

- Depth, size, volume
- Feature density
- Mobility (live cell)
- Observation time
- Bound/unbound fraction
- Out-of-focus blur
- Scattering
- Optical aberration

### System configuration (method choice)

- Objective choice: oil vs. silicon immersion
- Camera: CCD, EMCCD, sCMOS, redout mode
- Lasers, dichroics, emission filters

### Labeling & sample preparation

- ☐ Labelling method (IF, FISH, FPs)
- ☐ High specificity (e.g. antibodies)
- ☐ Sufficient brightness and photostability
- ☐ Low background / autofluorescence
- ☐ Optimal optical quality (embedding, aberration, cleanliness, accuracy)
- ☐ Fluorophore density

Kraus et al. 2017

## B System operation

### 1 Calibration / maintenance (specialist)

- ☐ Field illumination evenness
- ☐ Co-alignment of cameras (multi-camera systems)
- ☐ Line spacing and angles (+1 / 0 / -1 beam position)
- ☐ Z-illumination - focus plane alignment (top phase)
- ☐ Measure specific OTF sets (RI,  $\lambda$ , NA)

### 2 Raw data acquisition

- ☐ Select channel acquisition order
- ☐ Select imaging volume (xy-/z-dimension)
- ☐ Optimize exposure time and laser power
- Trade-off: dynamic range vs. photobleaching.
- Intensity fluctuations vs. drift; MCNR optimization
- ☐ Spherical aberration correction: select oil refractive index or use correction collar to adapt for temperature, imaging depth and refractive index mismatch

### 3 Reconstruction

- ☐ Select optimal OTFs
- ☐ Set high frequency (Wiener) filter
- ☐ Deactivate automatic cut-off
- ☐ Drift correction (rotary grating systems only)

## C Quality control



### 1\* Calibration tools (specialist)

- ☐ Raw Fourier projection
- ☐ Spherical aberration mismatch (ZMV)
- (RI-match / z-illumination optimization)
- ☐ Illumination pattern focus (+1 beam phase)
- ☐ Illumination phase steps (experimental systems)

### 2\* Raw data quality control

- ☐ Intensity profiles (bleaching, intensity variation)
- ☐ Raw Fourier projection
- ☐ Motion & illumination variation
- ☐ Modulation contrast to noise ratio (MCNR)

### 3\* Reconstructed data quality control

- ☐ Intensity histogram (max-to-min ratio; MMR)
- ☐ Spherical aberration mismatch (ZMV)
- ☐ Fourier plot analysis
- ☐ Modulation contrast map

Ball et al. 2015

## D Data postprocessing

### Image processing

- ☐ 3D channel alignment
- ☐ (Auto-)Clipping & 16-bit conversion
- ☐ MCN-filter (optional)

### Quantitative analysis

Segmentation, 3D centroids, nearest neighbor distribution, cluster analysis, cross-correlation ...

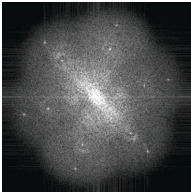
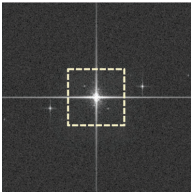
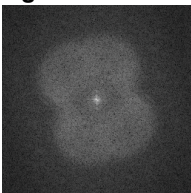
Kraus et al. 2017

Data storage & curation



**Supplementary Manual** | Checklist of specific steps for ensuring high-quality SIM results. **(a)** Experimental design considerations upstream of the imaging process. **(b)** Series of checks for the user or specialist to confirm before, during, and after data acquisition. **(c)** Functionalities in the SIMcheck plugin that can help diagnose the issues raised in the left column. **(d)** Post-processing steps down-stream of the imaging procedure for completeness. All or most boxes should be checked (meaning that the issue has been considered and a solution with rationale has been reached) before making substantial conclusions from SIM data.

**Supplementary Table** | Advanced artifact diagnostics for bespoke system setups

Artifact type	Likely cause	SIMcheck readout	Troubleshooting
<b>10 FFT extra dots in diagonals</b> 	Deviation from $2\pi/5$ phase shift at the image level. The failure in information separation of individual orders mixes up strong center bands in higher order	<i>Reconstructed Fourier Plot</i> Dots on the diagonals.  <i>[System calibration] Illumination Phase Steps</i> Measures the phase values of the bright spot at the 1st order after FFT of the raw images, can be used to check the phase steps are really $2\pi/5$ (assuming 5 phases per angle).	[System] Check stabilities of <ul style="list-style-type: none"> <li>the illumination intensity (including the fiber shaker in OMX v2-3)</li> <li>the sample/stage (including pressure of the vibration isolation table)</li> <li>temperature of cameras.</li> </ul> If the step sizes of the phases still differ from $2\pi/5$ , change voltages of piezo or galvo mirrors (requires service engineer).
<b>11 FFT reproducible dots</b> 	Extra beams due to unwanted reflection (stray light) in the optical path.	<i>Raw Fourier Projection</i> Reproducible spurious dots outside 1 <sup>st</sup> and 2 <sup>nd</sup> order stripe spots.	[System] Check for extra beams: remove objective, reduce illumination power to < 10%, open the shutter and project beams on a white surface on the ceiling. <b>(Caution:</b> only to be performed by a trained specialist. Do not look directly at laser light!) Optical alignment or installing apertures help to minimize it (requires service engineer).
<b>12 FFT uneven amplitude among angles</b> 	[System] Beam centering. Alternatively polarization is disrupted in a particular angle due to dichroic mirror or inaccurate K0 values. [Sample] Unequal refractive index or strong bleaching	<i>Raw Fourier Projection</i> Frequencies of 1 or 2 angles extend less far out.  Angle intensity variations of <30% are still acceptable.	[System] To check polarization, remove objective lens, reduce illumination power to < 1% and insert a polarizer to examine if the illumination intensity goes down as the polarizer is rotated. This problem is angle- and possibly wavelength-dependent. Exchange the dichroic mirror. [Sample] Check bleaching rate.

## **ADDITIONAL SUPPLEMENTARY MATERIALS**

### **REAGENTS**

- TetraSpeck Fluorescent Microspheres 0.2  $\mu\text{m}$  diameter (ThermoFisher, cat. no. T7280)
- Phytigel™ powder (Sigma, cat. no. P8169-100G)
- CyGEL™ (BioStatus)
- Silicon gasket (Harvard Apparatus)
- DPBS (Sigma, cat. no. D8537)
- Calcium Chloride (Sigma, cat. no. 10043-52-4)
- Magnesium Chloride (Gibco cat. no. 14040)
- Borosilicate precision cover glasses, thickness No. 1.5H ( $170 \pm 5 \mu\text{m}$ ); 18x18 mm or 22x22 mm (e.g., Marienfeld Superior, cat. no. 0107032)
- Quick-drying nail polish, preferably bright colored metallic, or CoverGrip coverslip sealant (Biotium, cat. no. 23005)

### **REAGENT SETUP**

- CyGEL is liquid when stored on ice and transitions to a gel at approx. 23 °C. PBS-primed CyGEL was prepared by adding 12.8  $\mu\text{l}$  of the supplied 40x PBS to a pre-cooled vial of CyGEL on ice. A pre-cooled pipette tip was used when mixing beads with the CyGEL to keep it in the liquid state until ready.
- Phytigel was prepared by adding 0.25 g of Phytigel™ powder (Sigma, P8169-100G) to 50 ml of rapidly stirring DPBS (plus Calcium Chloride and Magnesium Chloride, Gibco 14040). Microwaving (or autoclaving) the solution to 80-90 °C was required in order to fully dissolve the powder. The gel was cooled to 40-50 °C before adding the beads, then mixed with the beads before it solidified at around 32 °C.

### **NOTE**

- Bead suspensions were prepared in either CyGEL™ (BioStatus) or Phytigel™ (Sigma). The refractive index of CyGEL is reported by BioStatus to be 1.37 and the measured refractive index of this Phytigel preparation was 1.338.

**1|** Well slides for 3D bead samples are prepared by applying an 18 mm square section of a 100  $\mu\text{m}$  thick silicon gasket (Harvard Apparatus) to a pre-cleaned glass slide. A hole approximately 3 mm square is cut out of the gasket using a razor blade, to form a small well.

**2|** Rapidly suspend 4 microliters of 100 nm or 200 nm diameter TetraSpeck beads in 100  $\mu\text{l}$  of cold CyGEL or warm Phytigel, Immediately pipette approx. 50  $\mu\text{l}$  were immediately into the gasket well.

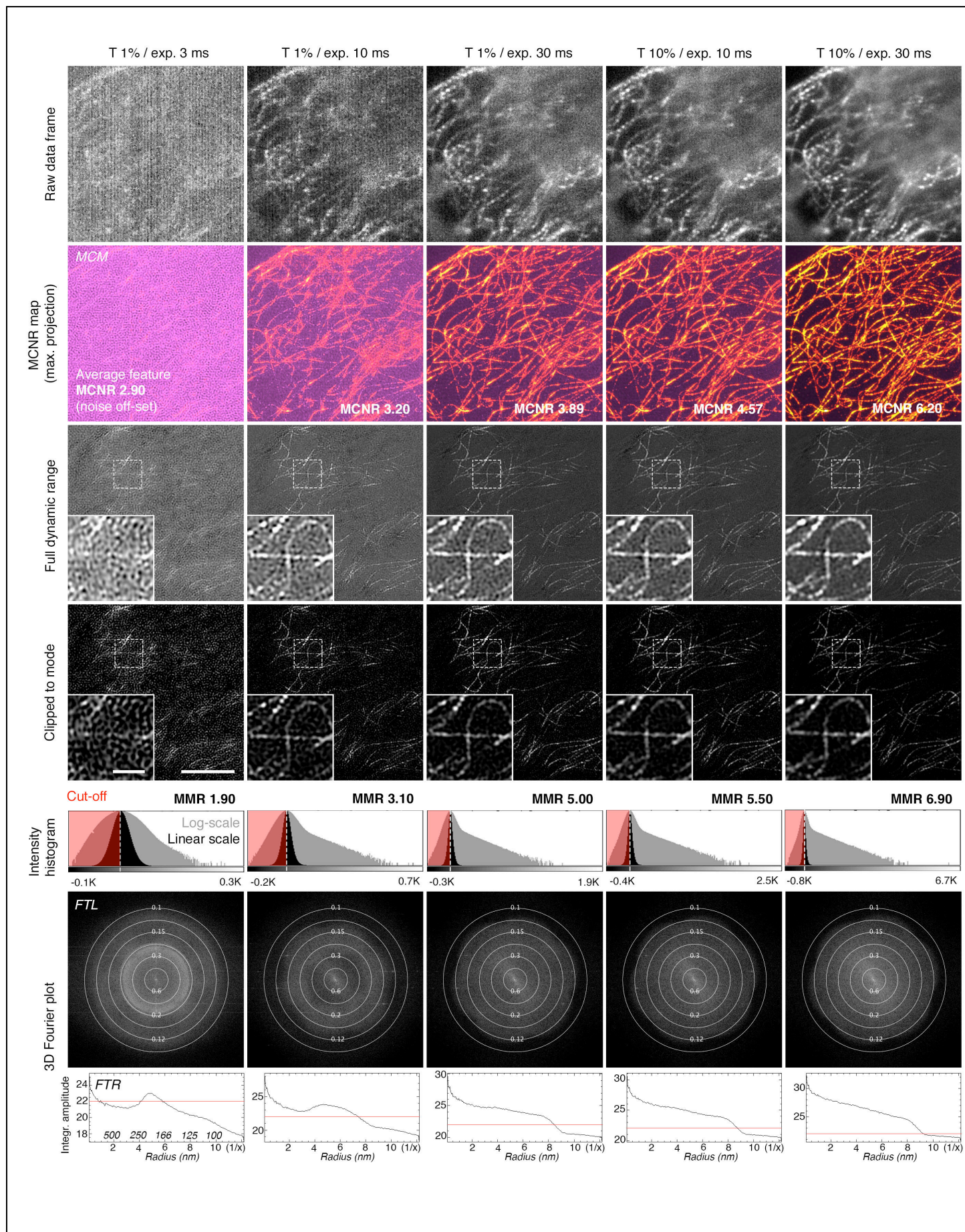
**▲ CRITICAL STEP** The 100 nm beads are more stringent for assessing spherical aberration, but the blue signal is easier to detect using 200 nm beads, therefore these were used for assessing chromatic shift.

**3|** Press a pre-cleaned high performance coverslip (18 mm square) firmly on top to extrude excess gel solution before it solidifies, to ensure the coverslip lays flat on the gasket.

**4|** Seal around the edges of the coverslip with quick-dry nail polish.

**▲ CRITICAL STEP** Gel slides should be stored at room temperature and used within 1-2 days of preparation to ensure that the gel does not dry out.



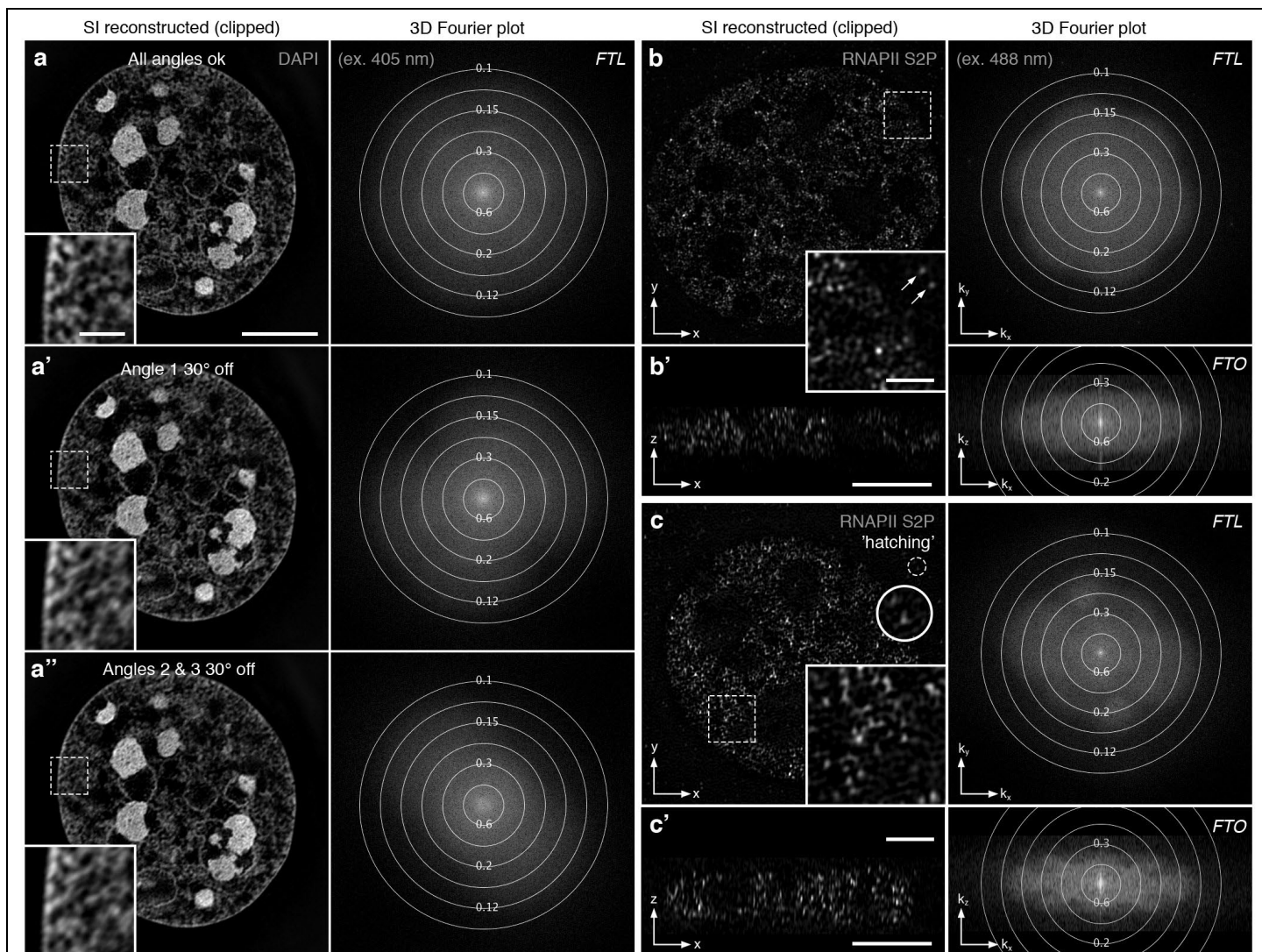


**Supplementary Figure 1**

## Reconstructed noise artifact as a function of modulation contrast in the SIM raw data

Datasets progress from having a very low signal-to-noise ratio (SNR) (far left column) up to an acceptable SNR (far right column) with initial acquisition conditions directly affecting quality of the resulting reconstruction. Data collected from wild type C127 mouse cells immunostained for tubulin (Alexa Fluor 488) are presented as: representative frames of raw datasets, with stripes shown in one angular direction (top row); modulation contrast to noise ratio (MCNR) in the raw data mapped onto the reconstructed dataset (MCN readout of *SIMcheck*; maximum projections; second row); reconstructed single-slice images showing the full dynamic range (third row); reconstructed single-slice images showing the dynamic range after cut-off below the mode value of the intensity histogram (fourth row). Reconstruction intensity histograms (fifth row) of reconstructed 32-bit data are shown as log-scaled (grey) or linear-scaled (black) intensity values, with the x-axis representing pixel intensity in the given range. The values removed in the mode-based cut-off overlaid in red, and the ratio between minimum and maximum values in the histogram (MMR) is expressed above each plot. Lateral 3D Fourier plots (*FTL*, sixth row) of the reconstructed data are shown with reciprocal distance in  $\mu\text{m}$  plotted as circles over the FFT. The radial profiles (*FTR*, last row) display the corresponding radially averaged amplitudes with the red line indicating a reference amplitude value (22, arbitrary units) for comparison. Note that with increasing signal-to-noise the profiles become smoother and the area between the reference and the curve become larger. For each image, the dashed box indicates the inset region. Scale bars: 5  $\mu\text{m}$  and 1  $\mu\text{m}$  (inset). For each row, T indicates % transmission of the 488 nm laser, and exp. indicates the exposure time. Images were acquired on a GE OMX V3 Blaze instrument with PCO edge 4.2 sCMOS cameras.

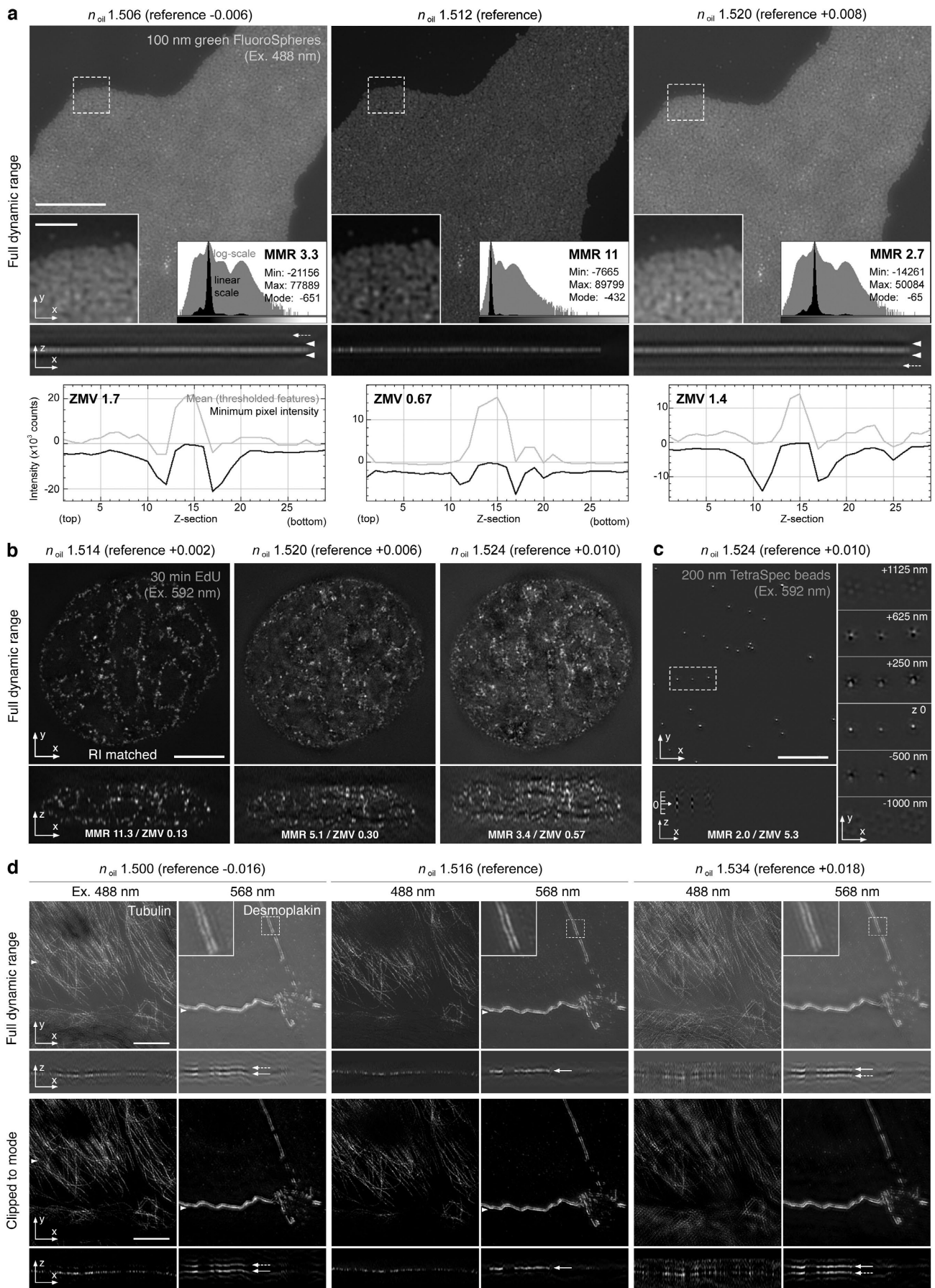




**Supplementary Figure 2**

### Illustration of 'hatching' artifacts caused by missing angle information

Data collected from wild type C127 mouse cells stained with either **(a)** DAPI to label chromatin distribution or **(b, c)** immunostained for RNA polymerase II phosphorylated at serine 2 of the C-terminal domain (RNAPII S2P). These showcase the effect of missing angular frequency information on complex (chromatin) or punctate (RNAPII) labeled features, supplementary to **Fig. 1c**. **(a-a'')** Reconstruction of the same dataset with correct angle ( $k_0$ ) settings **(a)**, and with a false  $k_0$  parameter settings for either one **(a')** or two **(a'')** angles, respectively. Note that the loss of lateral resolution enhancement is particularly evident in the corresponding Fourier plots with frequency extensions missing for the affected angles (second column). Accordingly, the labeled features in the reconstructed images (insets) are less sharp. **(b, c)** Reconstruction of punctate nuclear RNAPII signals with correctly fitted  $k_0$  value **(b)** compared to a dataset where the  $k_0$  fitting failed for two of the three angle directions **(c)**. Detailed view of the reconstructed lateral midsection highlight elongated features of nuclear signals in **c**, but not in **b** (boxed insets). Single cytoplasmic background signals (originating from unspecific bound antibody complexes) show 'starfish' extensions in the faulty dataset (circular inset in **c**) while similar signals are round in the well-reconstructed dataset (arrows, inset in **b**). While not easily noticeable in the reconstructed image, the absence or presence of hatching becomes apparent in the corresponding Fourier plot. Of note, enhancement of the axial resolution, as well as contrast increase by out-of-focus signal suppression are hardly affected, as highlighted by the comparison of the the orthogonal sections and the corresponding orthogonal Fourier plots in **b'** and **c'**. Scale bars: 5  $\mu\text{m}$  and 1  $\mu\text{m}$  (insets). Images were acquired on a GE OMX V3 Blaze instrument with PCO edge 4.2 sCMOS cameras.

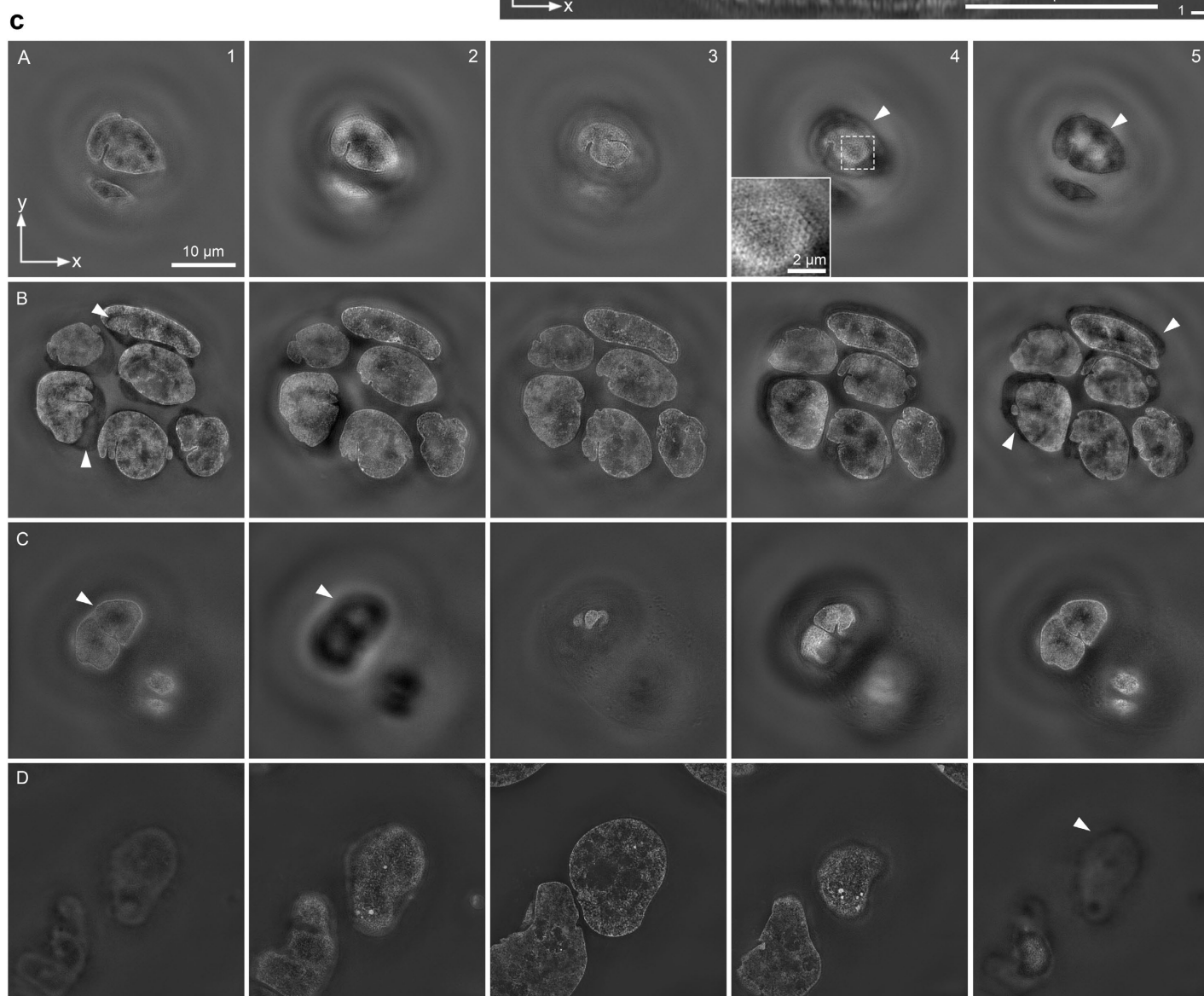
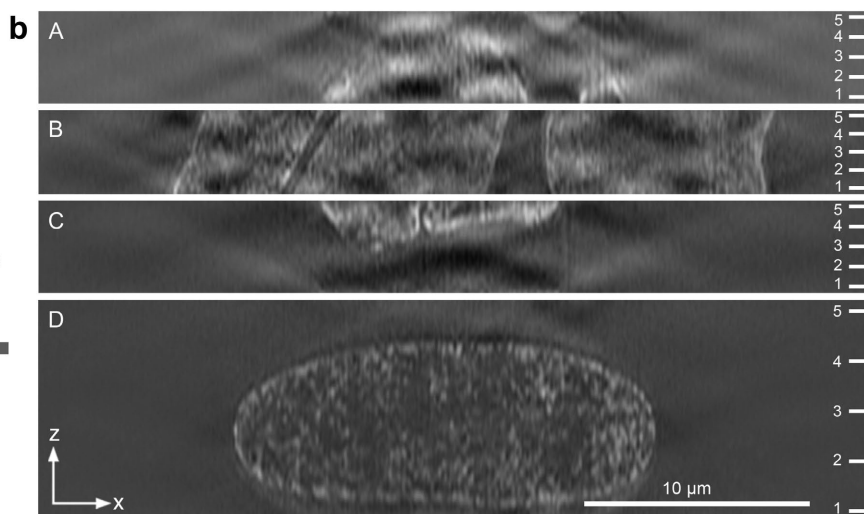
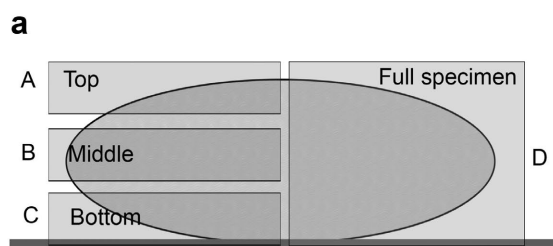


### Supplementary Figure 3

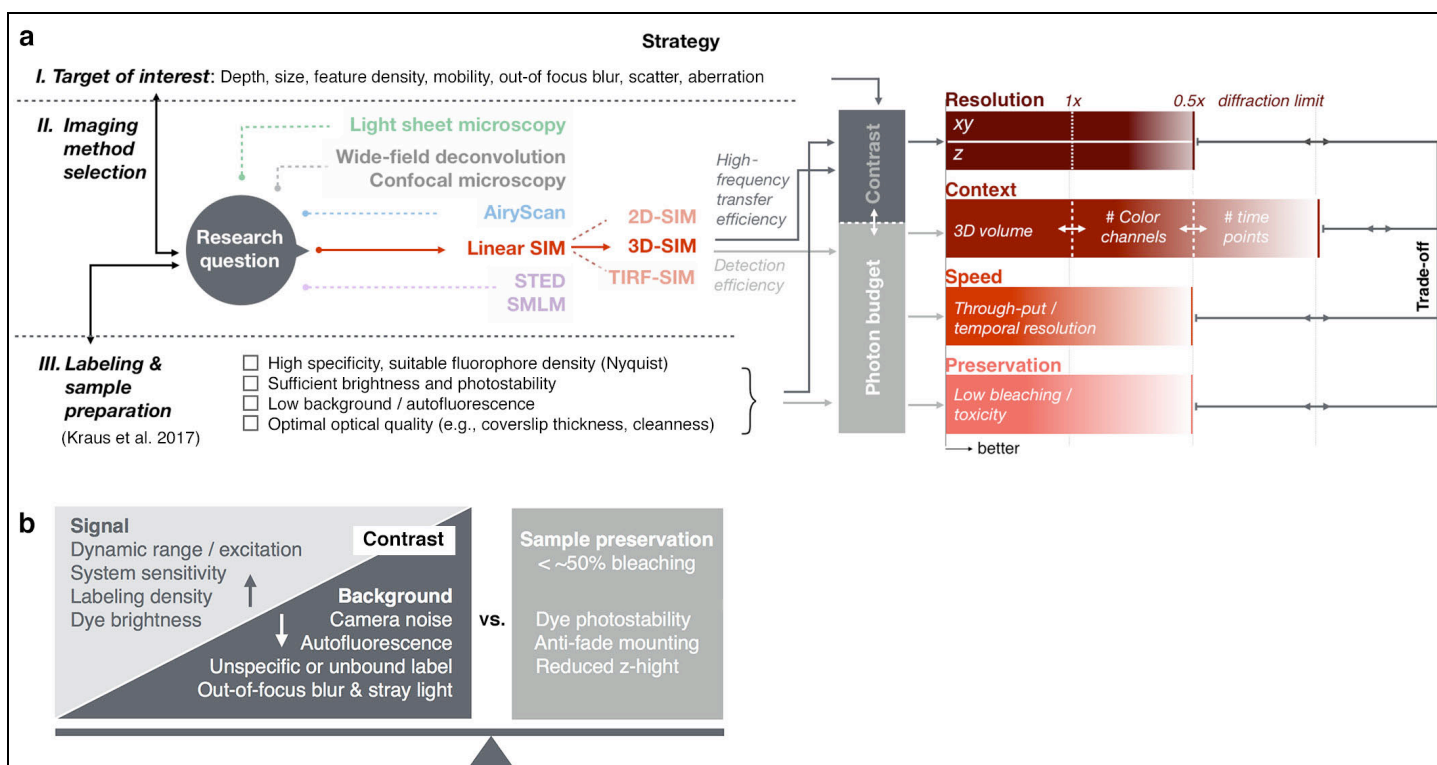
#### Illustration of refractive index mismatch induced artifacts

(a) Mounting medium refractive index (RI) matched to the sample will exaggerate or suppress the z-ghosting artifact, as observed in lateral and orthogonal views of sub-diffraction sized FluoSphere green (Ex. 488 $\lambda$ ) coverslip beads (*Ref.* calibration slide #1). As the acquisition medium's refractive index (RI) is varied from too low (left) to optimally matched (middle) to too high (right) reconstruction of the depicted area is seen to increase in quality nearest the sample's reference oil. Orthogonal views highlight that an extreme mismatch (>5 units change from reference RI) produces images with prominent intensity dips (arrowheads) in z-slices adjacent to sample real signal. Additionally, undershooting the sample's RI-match can result in a noticeable ghost image in z-slices atop real signal while overshooting this match results in a ghost image of beads repeated in z-slices beneath real signal (dotted arrows). (b) Effect of increasing RI mismatch on a punctate nuclear staining pattern (EdU pulse replication labeling and detection with click chemistry in C127 cells). Note the intermixing of real and ghost signals in the orthogonal views with increasing mismatch. (c) RI mismatch on very bright isolated features (here 200 nm diameter TetraSpeck beads) produces characteristic hexagonal patterns of the out-of-focus echo signal, highlighted in the detailed view of individual z-planes through a selected bead (right). (d) Image series supplementary to **Fig. 1e** demonstrating ghosting on an MDCK cell immunostained for tubulin (Alexa Fluor 488) and desmoplakin C-terminus (Alexa Fluor 568) to emphasize the ease in diagnosing intensity dips from an RI-mismatch in images prior to any thresholding. Upper row of panels shows the lateral (top panel) and orthogonal (bottom panel) cross section of the reconstructed dataset with the full dynamic range, while the lower row shows the same data after intensity cut-off at zero. Arrowhead (first column) indicates position of the orthogonal view. Scale bar: 5  $\mu$ m. Images in (a), (b), and (c) were acquired on a GE OMX V3 Blaze instrument with PCO edge 4.2 sCMOS cameras; images in (d) were acquired on a GE OMX V3 Blaze instrument with Photometrics Evolve EMCCD cameras.





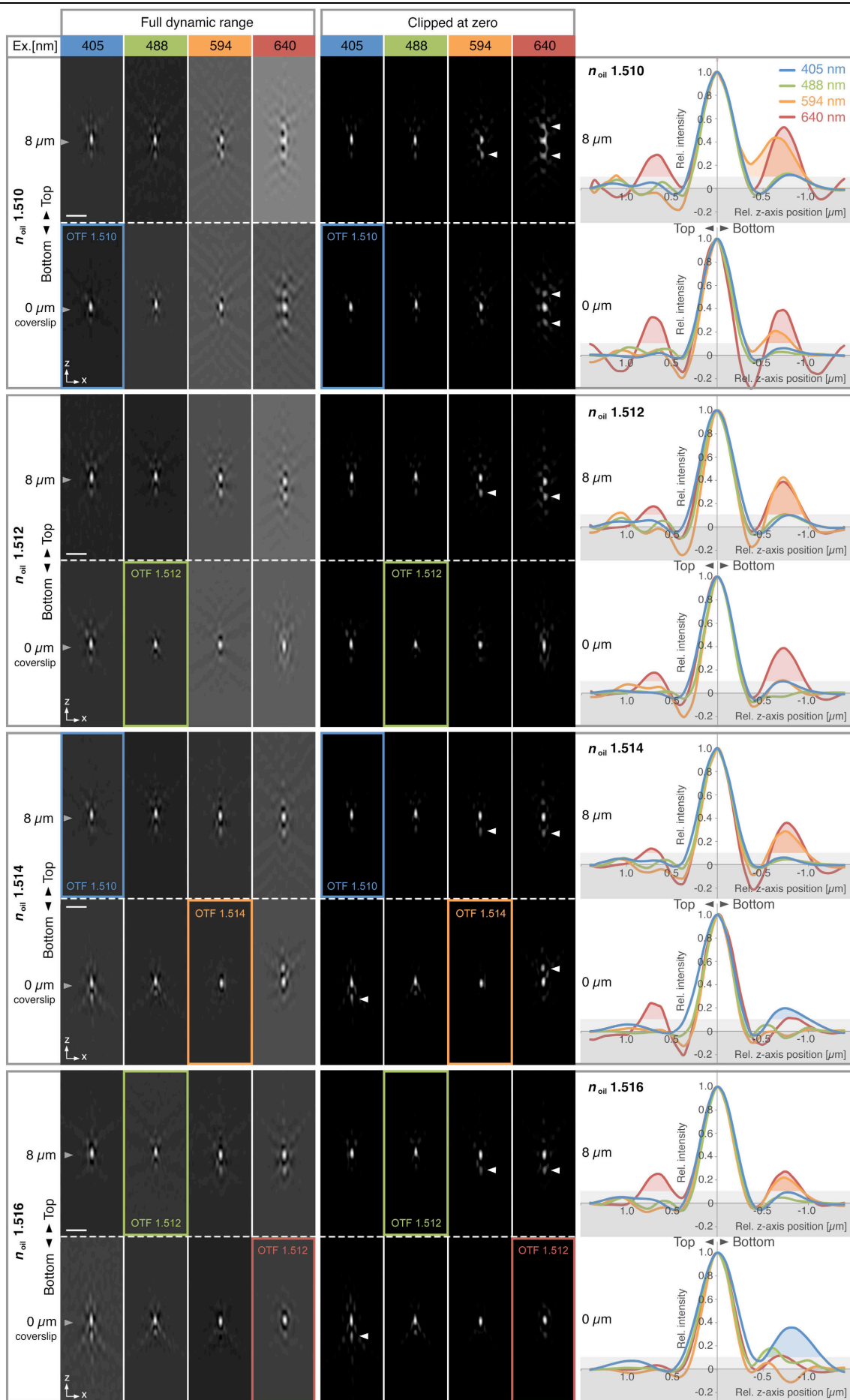
Supplementary Figure 4
<b>Illustration of z-wrapping artifacts</b>
<p>(a) Schematic diagram indicating the top (A), central (B), bottom (C), and full (D) sub-sections used for the reconstruction. Coverslip is on the bottom. (b) Orthogonal views of the resulting reconstructions. Note the artifactual patterns generated in (A) and (C) sections. Tick marks in each indicate positions of images shown in the next panel. (c) Representative slices of each reconstruction, corresponding to the z positions marked in (b). Letters represent the corresponding sub-section of the entire nucleus as shown in (a), while numbers represent the corresponding z-position shown in (b). Arrowheads denote z-wrapping artifacts, or ghost signals from other z-slices in the reconstructed segment that occur on the opposite end of a z stack to where the stack has finished acquisition on a prominent structural feature. These include shadowing and moderate 'honeycomb' patterning (inset). Bar: 10 <math>\mu\text{m}</math>, 2 <math>\mu\text{m}</math> (inset). Images were acquired on a GE OMX V3 Blaze instrument with PCO edge 4.2 sCMOS cameras.</p>

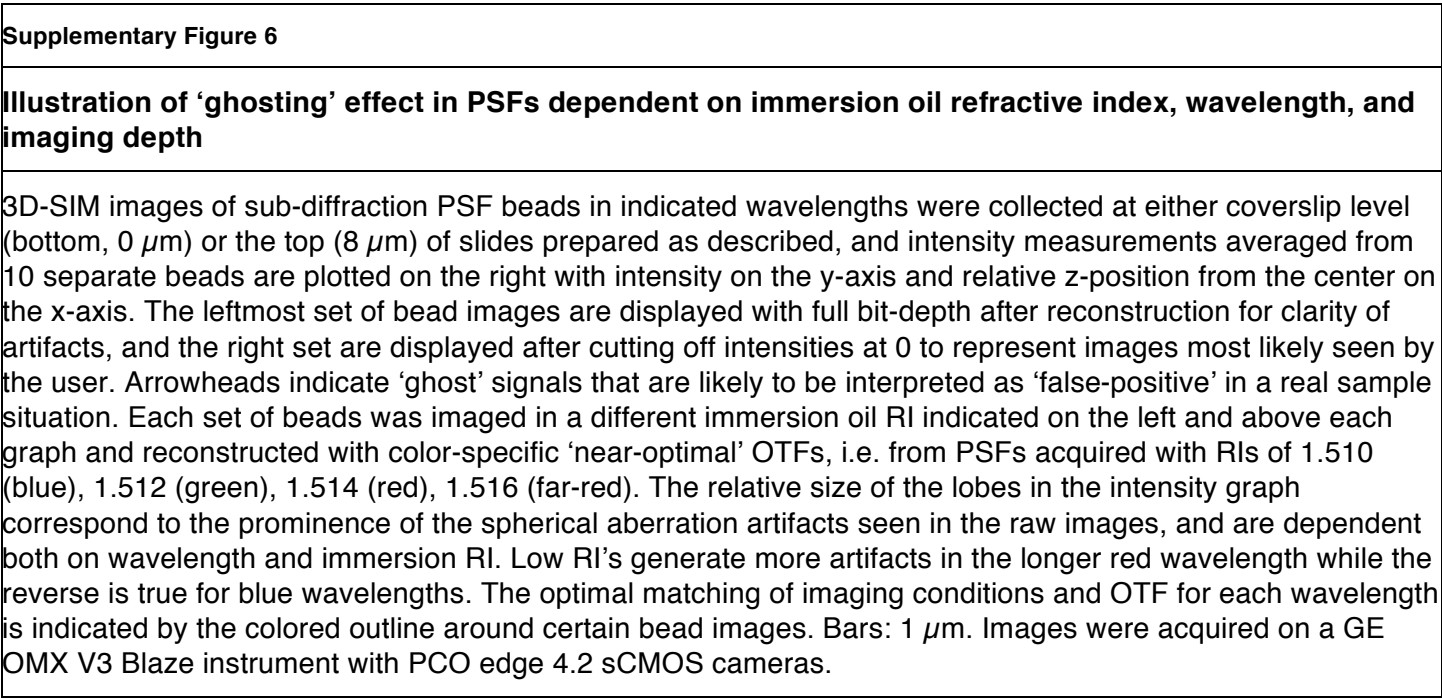


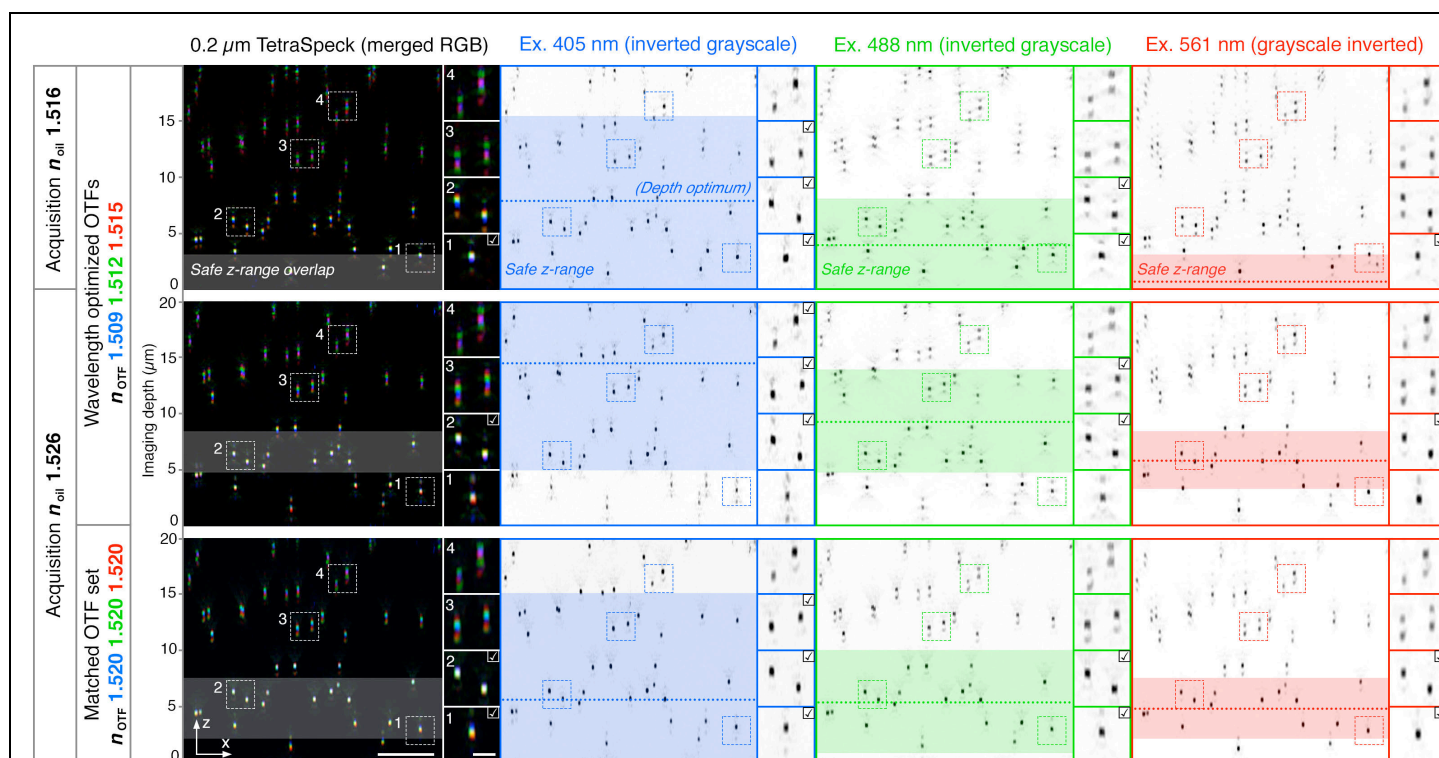
Supplementary Figure 5

## Strategic considerations for imaging method selection and trade-off finding

(a) Schematic diagram illustrating factors influencing the strategic decision of imaging modality selection and governed by the research question to be addressed. Also illustrated are the contributions of experimental factors affecting the relative balance between contrast and photon budget, and where these feed into technical considerations to optimize resolution, context, speed, and sample preservation. Note that improving one area will necessarily lead to trade-offs in others. (b) Schematic representation of potential factors increasing the signal and reducing unspecific background to increase the overall image contrast, which is balanced with photodamage and fluorophore bleaching not exceeding some critical threshold. Too much bleaching reduces SNR and thus the (modulation) contrast in the raw data, and will induce artifacts if the ratio is weighted too heavily towards generating high signal at the start of the dataset acquisition. The level of bleaching allowed depends on the acquisition order and may be case-dependent; however, from experience rates of up to 50% seem acceptable in most cases. The 'Channel Intensity Plot' function in *SIMcheck*<sup>13</sup> offers a useful tool for quantifying acquisition bleaching and intensity variations affecting SNR and modulation contrast in SIM raw data.





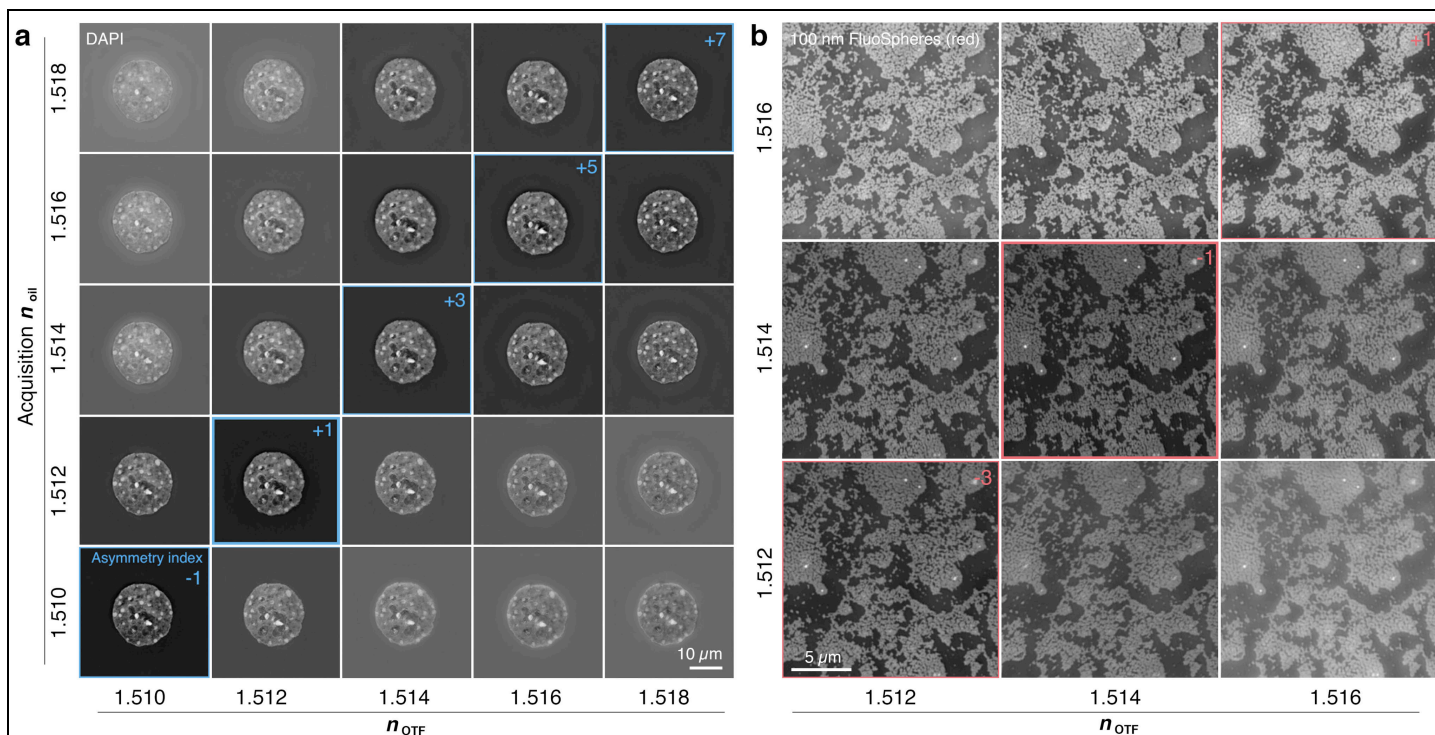


**Supplementary Figure 7**

### **SIM acquisition of 3D bead samples highlighting variations in the ‘safe z-range’ and color channel matching under different imaging conditions**

Comparisons of multicolour gel-embedded 200 nm TetraSpeck beads, imaged on a GE OMX V4/Blaze system (100x/1.40 SApo objective) using varying RI immersion oils (indicated on left) and reconstructed using different combinations of OTFs (coloured legends, also on left). The left image column shows xz-views (maximum projection) of superimposed channels (after image registration). The other columns show individual blue, green and red emission channels of the same xz-projections. In all images the coverslip is at the bottom and the y-axis shows ascending z-distance deeper into the gel. Insets show higher magnification views of individual beads with accompanying spherical aberration artifacts as a function of distance from the coverslip. Note the significant doubling/tripling of bead images in the xz-axis, especially when using an oil of too low RI (1.516) for this sample (top row). Superimposed images also reveal colour dispersion in the aberrated regions, particularly after reconstruction using channel-optimised OTFs (middle image row), rather than matched OTF sets (bottom row). Ghosting effects are most extensive in the red channel and least problematic in the blue channel. Dotted lines the depth optimum, colored areas around indicate the corresponding safe z-range, for each channel, i.e. the range of depths within which ghosting effects are minimal. The extent and z-position of the safe z-range varies with acquisition RI, wavelength, and the OTFs used for reconstruction. Details on assembling gel-embedded bead samples are available in **Supplementary Protocol 1**. Scale bars: 5  $\mu\text{m}$  and 0.5  $\mu\text{m}$  (inset). Images were acquired on a GE OMX V3 Blaze instrument with Photometrics Evolve EMCCD cameras.

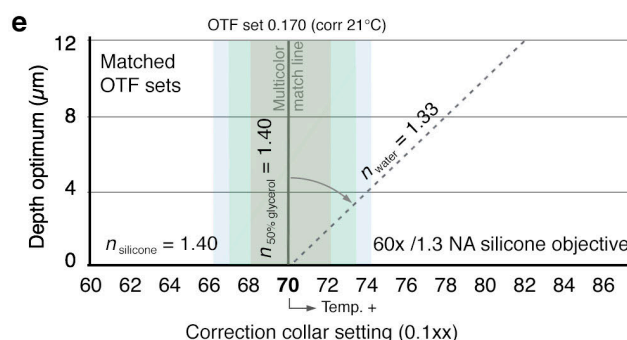
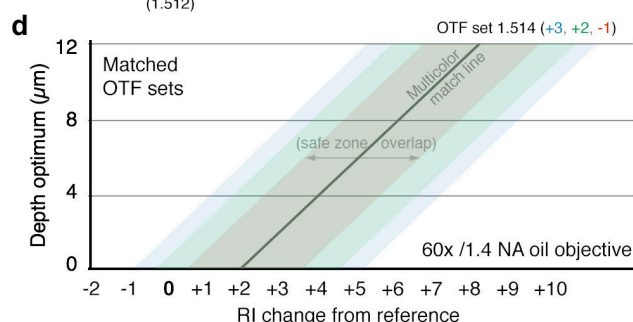
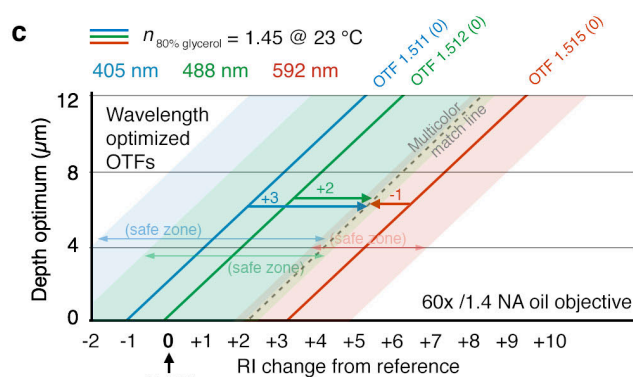
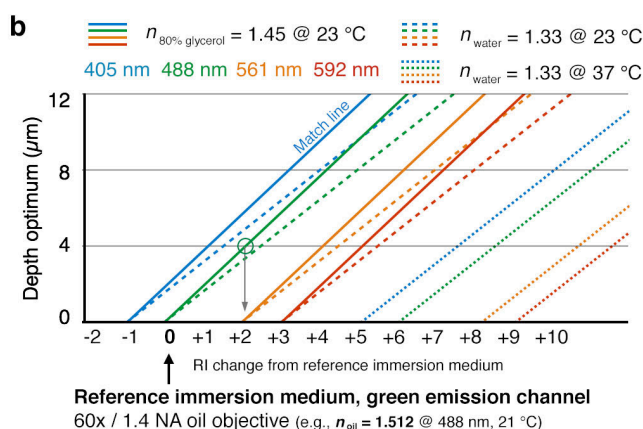
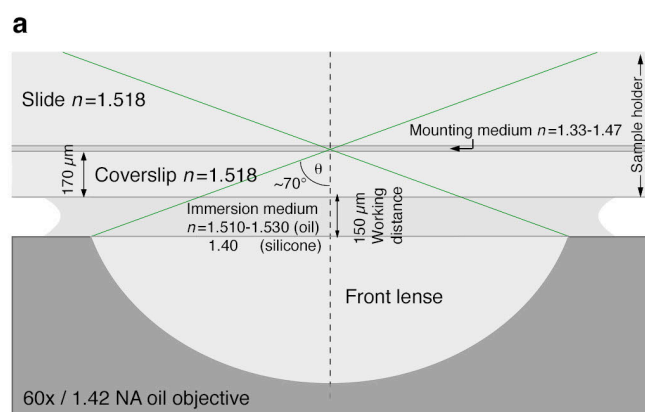




**Supplementary Figure 8**

### Matching of refractive indices of immersion oils used for sample acquisition and OTF measurements can compensate for PSF asymmetry

(a) Matrix of acquisitions of the same DAPI-stained C127 nucleus with varying immersion oil RIs (y-axis) reconstructed with OTFs generated from matching or varying immersion oil RIs ( $n_{OTF}$ , x-axis). Images are shown with full bit depth and no discarding of negatives to emphasize the dynamic range of the reconstruction. The immersion oil RI generating the most symmetrical PSF on the system used is 1.511, therefore the ‘asymmetry index’ is calculated as deviations from that metric based on the immersion RI used. This clearly shows that matching the immersion oil RI during acquisition of both the OTF and the raw image results in higher contrast and a better reconstruction than using an OTF generated with the ideal RI to reconstruct and image collected with a different immersion oil RI. (b) Example of 100nm red bead layer showing a similar effect. The extent of mismatch compensation, however, is affected by wavelength, as PSFs of longer wavelengths are more easily distorted than shorter wavelengths (prominence of side lobes, see **Supplementary Fig. 6**). Thus, matching refractive indices  $n_{oil}$  and  $n_{OTF}$  results in a smaller window of acceptable compensation. Scale bars: 10  $\mu m$  (a), 5  $\mu m$  (b). Images in (a) were acquired on a GE OMX V3 instrument with Cascade II:512 EMCCD cameras, and images in (b) were acquired on a GE OMX V3 Blaze instrument with PCO edge 4.2 sCMOS cameras.



Supplementary Figure 9

## Schematic representation of matching spherical aberrations of OTF and sample for multi-channel SIM imaging

(a) Representation to scale of the light path through sample components. For a high NA oil objective, the opening angle  $\Phi$  is approx.  $70^\circ$ . Fixed and variable refractive indices  $n$  of the different components are indicated. (b) Representation of determining optimal OTF sets based on sample depth (based on empirical data acquired on an OMX V3 Blaze system). The y-axis represents depth, or the distance of the sample region from the coverslip, in  $\mu\text{m}$ . The x-axis indicates the relative change in refractive index (RI) of the immersion oil from a pre-determined, system-specific reference – generally the RI of oil that gives a symmetrical PSF in the green channel at the coverslip. The optimal OTF for the 488 nm excitation channel on this system was determined (by observed symmetry of the PSF) to be at an immersion RI of 1.512 (defined as the zero point on the x-axis, as the reference value may deviate on other systems). These measurements are valid for samples mounted in glycerol with a RI of 1.47 at  $23^\circ\text{C}$ , with solid lines indicating the depth at which a given immersion RI will produce a symmetrical PSF in glycerol, and would thus best match to an OTF measured at the coverslip. E.g. following the green match line for 488 nm excitation, for best matching in  $4\mu\text{m}$  depth the RI should be increased by +0.002 relative to the reference (circle, grey arrow); in this particular case an oil with RI of 1.514 should be used. Dashed lines represent the equivalent values for water-based immersion media (such as Opti-MEM) at  $23^\circ\text{C}$ , and dotted lines represent equivalent values for water-based immersion media at  $37^\circ\text{C}$ . Note that the higher refractive index between immersion and mounting medium causes a stronger tilt along the y-axis, while a temperature increase effectively changes viscosity and thus the RI of the immersion oil,



leading to a deviation from the nominal RI typically indicated for 23 °C, and shifts along the x-axis. **(c, d)** Representations of the match lines and the corresponding safe z-ranges of good reconstruction quality when using color optimized OTFs **(c)** as compared to using a set of channel specific OTFs acquired with the same RI (in this example 1.514) shifting the optimum towards the red channel **(d)**. Note that in the latter case the match lines for all channels co-align and the corresponding safe zones display a much wider overlap region. **(e)** Representation of the ideal case of having no RI mismatch achieved when combining silicone oil immersion objective and a RI matched mounting medium (e.g. 50% glycerol), and both matching the RI of the biological specimen. Theoretically this would allow aberration-free imaging throughout the working distance of the objective. In praxis, however, light scattering and specimen-inherent RI variations will become limiting, especially when the light must penetrate through many layers of biological tissue, for which correction requires more advanced adaptive optics.



frequency space (arrowheads, right panel), highlighting that despite overall resolution being comparable to an aligned instrument (left), the misaligned instrument (right) is generating suboptimal SIM images. Images were acquired on a GE OMX V3 Blaze instrument with PCO edge 4.2 sCMOS cameras.